A first investigation of hydrogeology and hydrogeophysics of the Maqu catchment in the Yellow River source region.

Mengna Li[1,2], Yijian Zeng[2], Maciek W. Lubczynski[2], Jean Roy[3], Lianyu Yu[2], Hui Qian[1], Zhenyu Li[4], Jie Chen[1], Lei Han[5], Han Zheng[1], Tom Veldkamp[2], Jeroen M. Schoorl[6], Harrie-Jan Hendricks Franssen[7], Kai Hou[1], Qiying Zhang[1], Panpan Xu[1], Fan Li[4], Kai Lu[4], Yulin Li[4], Zhongbo Su[2]

[1]School of Water and Environment, Chang'an University, Xi'an 710054, China
[2]Faculty of Geo-Information Science and Earth Observation (ITC), University of Twente, Enschede, 7500 AE, The Netherlands
[3]IGP, Outremont, QC H2V 4T9, Canada
[4]Institute of Geophysics and Geomatics, China University of Geosciences, Wuhan, 430074, China
[5]School of Land Engineering, Chang'an University, Xi'an 710054, China
[6]Soil Geography and Landscape Group, Wageningen University, P.O. Box 47, NL-6700 AA Wageningen The Netherlands
[7]Forschungszentrum Jülich GmbH, Agrosphere (IBG-3), Jülich, 52425, Germany

Correspondence to: Zhongbo Su (z.su@utwente.nl), Yijian Zeng (y.zeng@utwente.nl) and Hui Qian (qianhui@chd.edu.cn)

Abstract. The Tibetan Plateau is the source of most of Asia's major rivers and has been called the Asian Water Tower. Detailed knowledge of its hydrogeology is paramount to enable the understanding of groundwater dynamics, which plays a vital role in headwater areas like the Tibetan Plateau. Nevertheless, due to its remoteness and the harsh environment, there is a lack of field survey data to investigate its hydrogeology. In this study, borehole core lithology analysis, altitude survey, soil thickness measurement, hydrogeological survey, and hydrogeophysical surveys (e.g., Magnetic Resonance Sounding – MRS, Electrical Resistivity Tomography – ERT, and Transient Electromagnetic – TEM) were conducted in the Maqu catchment within the Yellow River Source Region (YRSR). The soil thickness measurements were done in the western mountainous area of the catchment, where hydrogeophysical surveys were difficult to be carried out. The results indicate soil thicknesses are within 1.2 m in most cases, and the soil thickness decreases as the slope increases. The hydrogeological survey reveals that groundwater flows from the west to the east, recharging the Yellow River. The hydraulic conductivity ranges from 0.2 m/d to 12.4 m/d. The MRS soundings results, i.e., water content and hydraulic conductivity, confirmed the presence of unconfined aquifer in the flat eastern area. The depth of the Yellow River deposits was derived at several places in the flat eastern area based on TEM results. These survey data and results can contribute to integrated hydrological modeling and water cycle analysis to improve a full–picture understanding of the water cycle at the Maqu catchment in the YRSR. The raw data set is freely available at https://doi.org/10.17026/dans-z6t-zpn7 (Li et al., 2020).

Deleted: [3]
Deleted: Zeng[1]
Deleted: Lubczynski[1]
Deleted: Roy[2]
Deleted: Yu[1]
Deleted: Qian[3]
Deleted: Chen[3]
Deleted: Veldkamp[1]
Deleted: Hou[3]
Deleted: Zhang[3]
Deleted: Xu[3]
Deleted: Su[1]
Deleted: Faculty of Geo-Information Science and Earth Observation (ITC), University of Twente, Enschede, 7500 AE, The Netherlands …
Deleted: IGP, Outremont, QC H2V 4T9, Canada
Deleted: School of Water and Environment, Chang'an University, Xi'an 710054, China
Deleted: be used to develop
Formatted: Font color: Auto
Formatted: Font color: Auto
Formatted: Font color: Auto

1 Introduction

With a huge amount of water storage, the Tibetan Plateau (TP) acts as the "Water Tower of Asia" (Qu et al., 2019; Wang et al., 2017), recharging many major Asian rivers including the Salween, Mekong, Brahmaputra, Irrawaddy, Indus, Ganges, Yellow, and Yangtze rivers (Immerzeel et al., 2009), feeding more than 1.4 billion people (Immerzeel et al., 2010), and promoting regional social and economic development (Xiang et al., 2016). Due to climate change, the TP has experienced accelerated temperature rise over the past decades (Huang et al., 2017). Since the 1950s, the warming rate over the TP ranges between 0.16 °C – 0.36 °C per decade, and rises to 0.50 °C – 0.67 °C per decade from the 1980s (Kuang and Jiao, 2016). The retreating glaciers and snow cover, decreasing wetland area, and rising snow lines indicate that the hydrological system on the TP is undergoing profound changes (Kang et al., 2010; Xu et al., 2016; Yao et al., 2013; Zhao et al., 2004).

So far, the groundwater-related studies on the TP are mainly satellite-based, focusing on using GRACE to estimate terrestrial water storage, which consists of surface water and subsurface water (Haile, 2011; Jiao et al., 2015; Zhong et al., 2009). Among those studies, Xiang et al. (2016) separated the groundwater storage from terrestrial water storage observed by GRACE using hydrological models and a glacial isostatic adjustment model.

An integrated surface-groundwater model is essential for improving the understanding of different processes quantitatively (Graham and Butts, 2005). To set up an an integrated surface-groundwater model, different kinds of data are needed for parameterization of land surface and subsurface, for atmospheric forcing, and state variables are required for model calibration and validation. Land surface data such as topography, land cover, and soil parameters can be obtained from Digital Elevation Models (DEMs) and regional or global soil databases (Su et al., 2011; Zhao et al., 2018). Atmospheric forcing data, including precipitation, air temperature, wind velocity, and other variables, are available from regional or global meteorological datasets (Su et al., 2013; Yang, 2017). However, subsurface data, like hydrogeological information (i.e., lithology, water table depth, hydrogeological parameters) and state variables (i.e., hydraulic heads and soil moisture content), usually require in situ measurements. These hydrogeology–related data are usually the most difficult ones to acquire, particularly considering the remoteness and harsh environment of TP (Yao et al., 2019).

Efforts have been made to develop the global map of permeability (Gleeson et al., 2014; Gleeson et al., 2011), hydraulic conductivity (Gupta et al., 2020; Montzka et al., 2017), groundwater table depth (Fan et al., 2013), groundwater volume and distribution (Gleeson et al., 2016). Nevertheless, due to the remoteness and harsh environment over TP (Yao et al., 2019), the above studies lack reliable in situ data in TP.

The conventional way to acquire hydrogeological information in an unknown area is by drilling boreholes and carrying out hydraulic tests, for example, pumping tests (Vouillamoz et al., 2012). However, due to the harsh environment of the TP, and the high costs and time–consuming of the traditional hydrogeological survey methods, little work has been done on the TP.

The hydrogeophysical methods are up-and-coming in hydrogeological studies (Chirindja et al., 2016). They have been applied in various conditions, for example in: wetlands (Chambers et al., 2014), rivers (Steelman et al., 2015), proglacial moraine (McClymont et al., 2011), karst regions (McCormack et al., 2017), and volcanic systems (Di Napoli et al., 2016; Fikos et al.,

Formatted: Font color: Auto

Deleted: An Integrated Hydrological Model (IHM), integrating groundwater with surface and above surface water fluxes,

Deleted: IHM

Formatted: Font color: Auto

2012). Compared to other hydrogeophysical methods, such as seismics, gravity and resistivity method, Magnetic Resonance Sounding (MRS) is the only method that is able to detect the free water in the subsurface directly (Lubczynski and Roy, 2003; Lubczynski and Roy, 2004), and quantify hydrogeological parameters and water storage (Lachassagne et al., 2005; Legchenko et al., 2002; Legchenko et al., 2018; Lubczynski and Roy, 2007). The MRS excitation is done at the earth's magnetic field. Therefore it depends on the subsurface resistivity. The electrical resistivity measurement is suggested to be jointly used with MRS (Braun and Yaramanci, 2008; Descloitres et al., 2007; Vouillamoz et al., 2002). Electrical Resistivity Tomography (ERT) is one of the predominantly employed hydrogeophysical methods to estimate the subsurface electrical resistivity (Herckenrath et al., 2012; Jiang et al., 2018). It has been widely applied together with MRS to explore regional hydrogeology (Vouillamoz et al. (2003), Descloitres et al. (2008), Pérez-Bielsa et al. (2012)). The Transient Electro-Magnetic survey (TEM), also referred to as the Time-Domain Electromagnetic Method (TDEM) in the literature, provides subsurface resistivity, but is able to achieve deeper penetration than ERT. On the TP, Gao et al. (2019) and You et al. (2013) used ERT to investigate permafrost. Nevertheless, there has not been any work done on the TP in terms of joint use of MRS, TEM, and ERT for hydrogeological surveys.

Investigations on various fields, such as geomorphology, climate change, glacier, and permafrost have been done on the TP based on different DEMs. Zhang et al. (2006) analyzed the geomorphic characteristics of the Minjiang drainage basin with SRTM (Shuttle Radar Topography Mission) data. Wei and Fang (2013) assessed the trends of climate change and temporal-spatial differences over the TP from 1961–2010, with a generalized temperature zone–elevation model and SRTM. Ye et al. (2015) calculated the glacier elevation change in the Rongbuk catchment from 1974 to 2006 based on topographic maps and ALOS. Niu et al. (2018) mapped permafrost distribution throughout the Qinghai–Tibet Engineering Corridor based on ASTER Global DEM. However, different DEMs used in different studies may lead to potential inconsistencies for understanding relevant physical processes. For Maqu catchment, it is crucial to understand the accuracy of different DEMs, since it controls the flow field of groundwater in this mountainous region. Therefore, we evaluate the accuracy of DEMs with a Real-time Kinematic-Global Positioning System (GPS-RTK), which has not been given attentions in many studies over the TP.

This study jointly uses hydrogeological and hydrogeophysical methods, including aquifer tests, MRS, ERT, TEM, and other necessary approaches at Maqu catchment in the Yellow River Source Region (YRSR) on TP. The paper is focusing on field hydrogeological and hydrogeophysical surveys, and corresponding datasets, aiming to fill the scientific and data gap in TP from a global view. Setting up a hydrogeological conceptual model will be presented in another paper. In what follows, the study area is introduced in Sect. 2. Borehole core lithology analysis, altitude survey, soil thickness measurement, hydrogeological survey, and hydrogeophysical survey are presented in Sect. 3. The results are documented and discussed in Sect. 4. Data availability is given in Sect.5. Conclusions are made in Sect. 6.

Formatted: Font color: Auto

Deleted: Some investigations have been done on the TP based on existing DEMs

Formatted: Font color: Auto

Formatted: Font color: Auto

Formatted: Font color: Auto

Formatted: Font color: Auto

Deleted: However, before applying DEMs, it is essential to evaluate the accuracy of DEMs with a Real-time Kinematic-Global Positioning System (GPS-RTK), which has not been given attention in many studies over the TP.

Deleted: The paper is focusing on the data part

2 Study area

The study area is a catchment (33°43′ N – 33°58′ N, 101°51′ E – 102°16′ E) in Maqu county, China. It is located at the northeastern edge of the TP, the first major bend of the Yellow River. Maqu is regarded as the "reservoir" of the YRSR. The length of the Yellow River passing through Maqu is 433.3 km. When the Yellow River flows through Maqu county, the annual runoff increases by 10.8 billion m^3, accounting for 58.7% of the total runoff of 18.4 billion m^3 of the Yellow River in the YRSR (Wang, 2008). The Maqu catchment is characterized by a cold climate with dry winter and warm summer (Dwb) in the updated Köppen–Geiger climate classification (Peel et al., 2007). The annual mean temperature is about 1.8 °C, and the precipitation is around 620mm annually. The catchment is covered by short grasses used for grazing by yaks and sheep. The elevation ranges between 3367 to 4017 m.a.s.l. according to ALOS PALSAR RT1.

Based on the field survey of geomorphology and geology, the catchment can be divided into two parts, the flat eastern area and the western mountainous area. The western mountains are feldspathic quartzose sandstone and sandy slate with soil covered at the top. While in the east part, the sediments are mainly alluvial deposits with intercalated eolian units. It is a high energy environment in which water is moving fast and able to carry particles of large grain sizes. The eastern part, together with its extension outside of the study area, is called the Ruoergai Basin. Surface processes cause erosion, mixing, unmixing, and redistribution of alluvial materials within the thick alluvia accumulation on the Eastern part. Geomorphological characterization was carried out in the Maqu catchment in 2018, and three terraces were identified (Fig. 1).

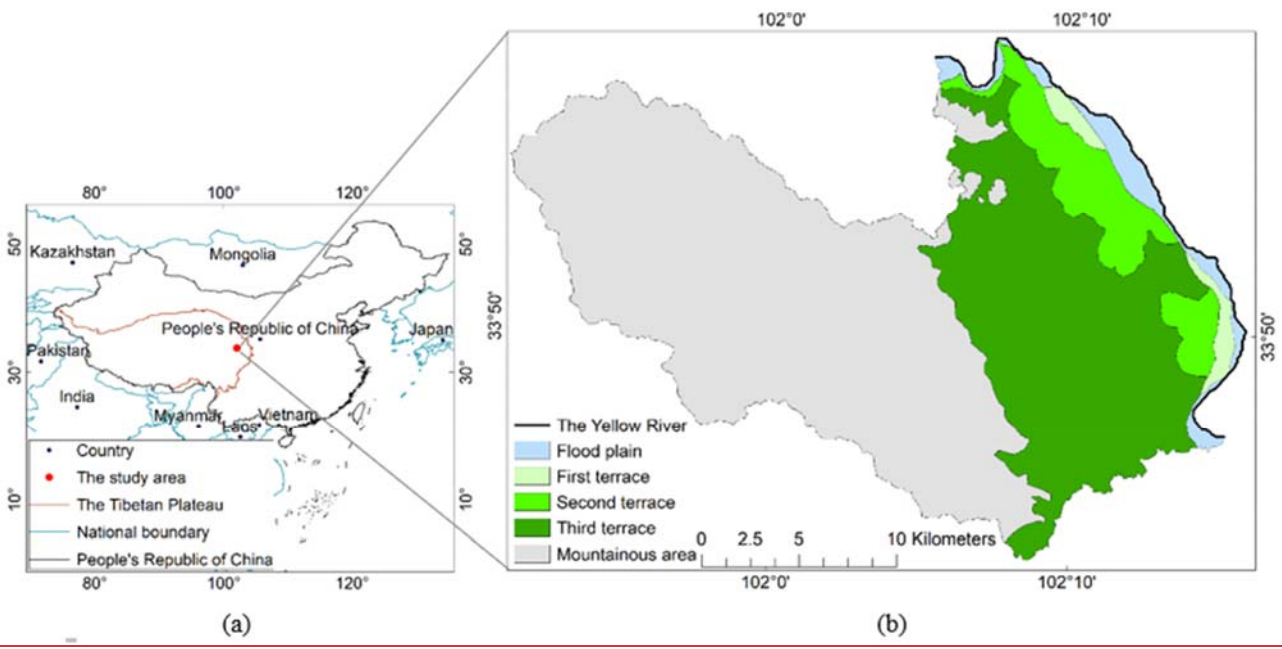

Figure 1. The geographical location of Maqu catchment in the TP and geomorphologic map: (a) The geographical location and boundary of the TP (Zhang et al., 2014a; Zhang et al., 2014b), and the geographical location of Maqu catchment; (b) The geomorphologic map of Maqu catchment.

Formatted: Font color: Auto

Formatted: Font color: Auto

Formatted: Font color: Auto

Formatted: Font color: Auto

Deleted: In terms of geomorphology and geology

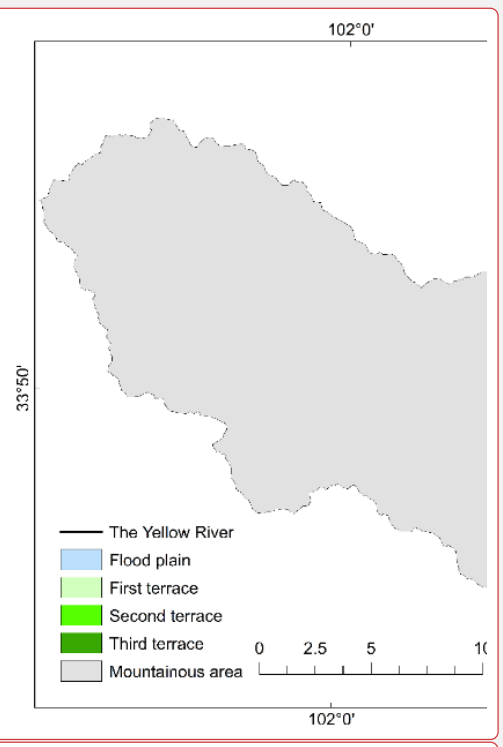

Deleted:

Formatted: Font color: Auto

Formatted: Font color: Auto

Formatted: Font color: Auto

Formatted: Font color: Auto

Formatted: Font color: Auto

Formatted: Font color: Auto

Formatted: Font color: Auto

Some previous works have been done in or around the catchment. Su et al. (2011) monitored the soil moisture and soil temperature from 5 to 80 cm below the ground surface. Dente et al. (2012) assessed the reliability of AMSR-E and ASCAT soil moisture products. Zheng et al. (2016) investigated the impacts of Noah model physics on catchment-scale runoff simulations. Zeng et al. (2016) combined the in situ soil moisture networks with the classification of climate zones to produce the in situ measured soil moisture climatology at the plateau scale. Zhao et al. (2018) studied the soil hydraulic and thermal properties of the 0.8 m top soil column. Zhuang et al. (2020) blended the surface soil moisture data from satellites, land data assimilation, and in–situ measurements with the constraint of in–situ data climatology, and estimated the root zone soil moisture by scaling the blended surface soil moisture product. The present research focuses on the hydrogeological and hydrogeophysical aspects, complementing previous studies.

Deleted: Figure 1. The geographical location of Maqu catchment in the TP and geomorphologic map.¶

3 Materials and methods

Formatted: Font color: Auto

Figure 2 shows the fieldwork workflow towards establishing a hydrogeological conceptual model, which includes the borehole core lithology analysis, altitude survey, soil thickness measurement, hydrogeological survey, and hydrogeophysical survey (Table 1 and Fig. 2). Yellow boxes in Fig. 2 represent the fieldwork, green boxes represent the results of fieldwork, which finally contribute to the hydrogeological conceptual model shown in a blue box. The obtained information on lithology, soil thickness, and elevation provides basic knowledge in the study area. Hydrogeological measurements of water table depth and hydraulic conductivity provide important input that can be used to deduce the direction and rate of regional groundwater flow. For hydrogeophysical results, magnetic susceptibility ensures the suitability of applying MRS, which provides information on water content and transmissivity. Furthermore, ERT not only provides information on underground resistivity but also integrated with MRS for retrieving water content and transmissivity. The locations of the surveys and measurements are shown in Fig. 3 and Fig. 4.

Deleted: Figure 2 shows the fieldwork workflow towards establishing a hydrogeological conceptual model, which includes the borehole core lithology analysis, altitude survey, soil thickness measurement, hydrogeological survey, and hydrogeophysical survey (Table 1 and Fig. 2). Borehole core lithology was analyzed in 2017. Altitudes were surveyed in 2019. Soil thicknesses were measured in both 2018 and 2019. The hydrogeological survey was carried out during 2017, 2018, and 2019, including water table depth measurements and aquifer tests. The hydrogeophysical survey was conducted in 2018 and 2019, deploying magnetic susceptibility measurements with magnetic susceptibility meter, resistivity measurement with ERT and TEM, and water content and transmissivity measurement with MRS. The locations of the surveys and measurements are shown in Fig. 3 and Fig. 4.

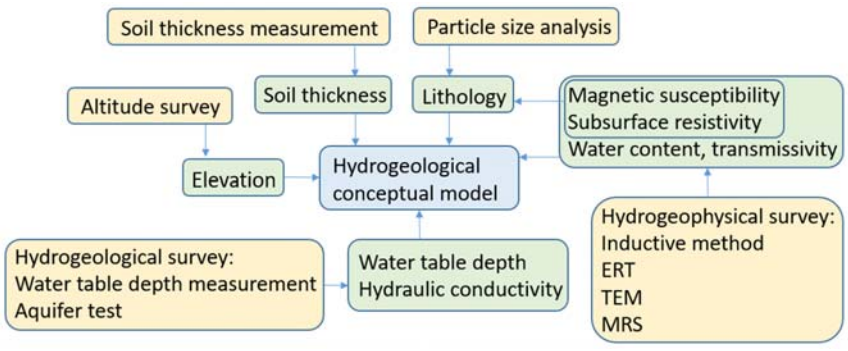

Figure 2. Fieldwork workflow for setting up a hydrogeological conceptual model at Maqu catchment.

Table 1. Methods, equipment, and timing for carrying out relevant measurements as in Figure 2.

Item		Method	Equipment	Time	Number of measurements	Source
Borehole core lithology		Particle size analysis	Sieve	2017	1	Well Report
Altitude		GPS-RTK	CHCNAV T4	2019	46	fieldwork
Soil thickness		Sampling	Auger, clinometer	2018,2019	77	fieldwork
Hydrogeological survey	Water table depth	Manual	Dipper	2018,2019	40*	fieldwork
	Hydraulic conductivity	Aquifer tests	Logger (3001–M10 Levelogger Edge and TD–Diver), pump, slug	2017,2019	11	fieldwork
Hydrogeophysical survey	Magnetic susceptibility	Inductive method	SM–20	2019	11	fieldwork
	Subsurface resistivity	ERT	WGMD–9	2018	7	fieldwork
		TEM	TEM–FAST–48	2019	10	fieldwork
	Water content, Transmissivity	MRS	Numis Poly	2018	18*	fieldwork

* sporadic measurements, not time series.

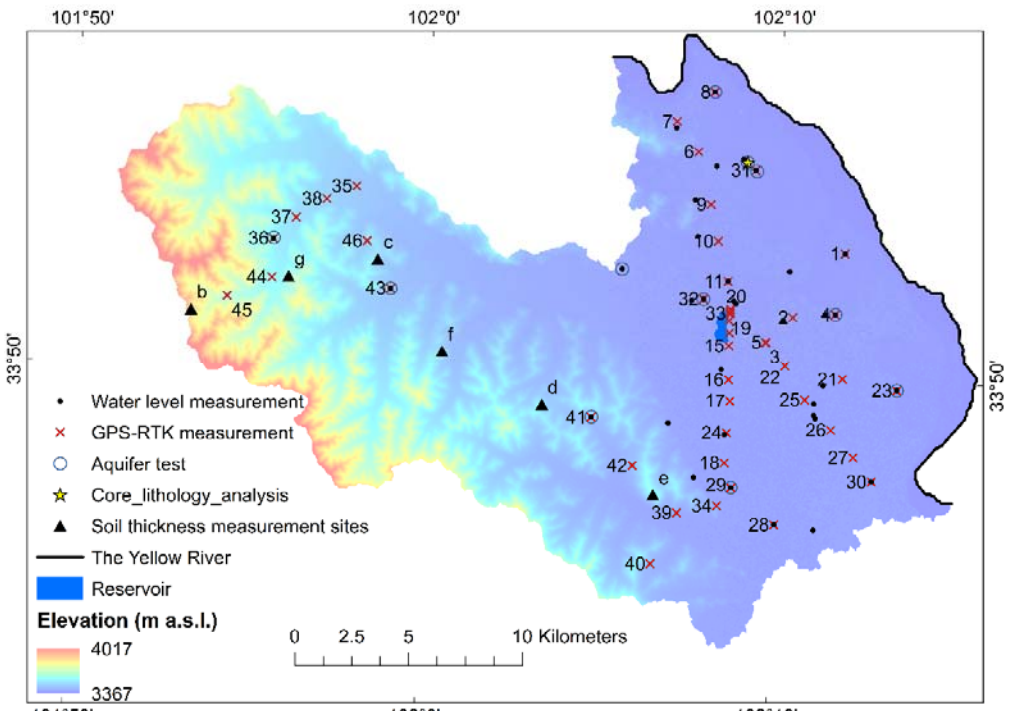

(a)

(b) (c) (d) (e) (f) (g)

190 **Figure 3.** Hydrogeological surveys, elevation measurements, and soil thickness measurements. (a) Locations of the hydrogeological surveys, elevation measurements, and soil thickness measurements. (b), (c), (d), (e), (f), and (g) are the exact locations of soil thickness measurements at sites b, c, d, e, f, g, respectively shown in (a), in the *.KML formatted image from © Google Earth. The numbers from 1 to 46 (due to limited space, several numbers are not shown in the figure) indicate the measurement sequence of GPS-RTK, and the sequence from b to g indicates the measurement sequence of soil thickness.

Formatted: Font color: Auto

Formatted: Font color: Auto

Deleted: (a) Locations of the hydrogeological surveys, elevation measurements, and soil thickness measurements. (b), (c), (d), (e), (f), and (g) are the exact locations of soil thickness measurements at sites b, c, d, e, f, g, respectively shown in (a), in the *.KML formatted image from © Google Earth. The numbers from 1 to 46 (due to limited space, several numbers are not shown in the figure) indicate the measurement sequence of GPS-RTK, and the sequence from b to f indicates the measurement sequence of soil thickness.

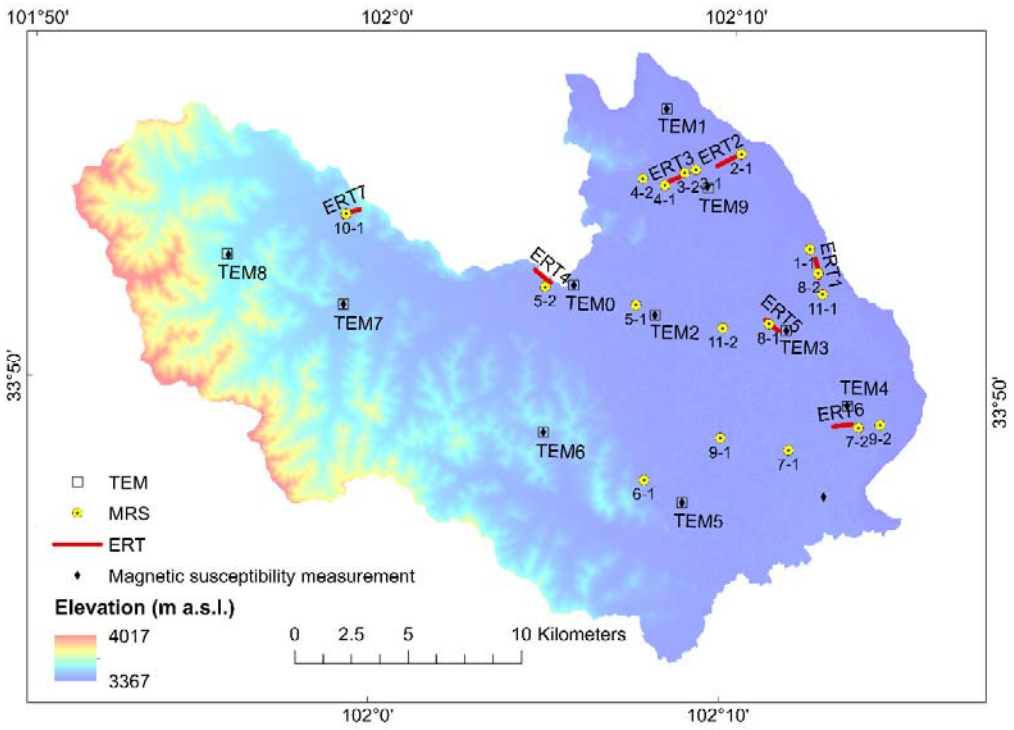

Figure 4. Location of hydrogeophysical surveys.

3.1 Borehole core lithology

The borehole core lithology is helpful in terms of understanding the formation of the area and estimating hydrogeological parameters. Some boreholes are available for water table depth measurement in the study area, but information of borehole core lithology is only available in one borehole ITC_Maqu_1 (Fig. 3a) drilled in 2017 down to the depth of 32 m from the ground surface. According to the borehole report, the lithology of the core was determined based on particle size analysis using the sieving method. Samples were analyzed using sieves with mesh sizes of 60, 40, 20, 10, 5, 2, 1, 0.5, 0.25, and 0.075 mm.

3.2 Altitude survey

The accuracy of ground surface elevation is crucial for the assessment of hydraulic heads, hydraulic gradient, and also groundwater flow and its direction, therefore it is also important for groundwater modeling. As a dynamic type of GPS positioning technique, GPS-RTK is able to achieve point position and elevation with centimeter-level accuracy in real-time. GPS-RTK instrument CHCNAV T4 from Shanghai Huace Navigation Technology Limited (https://www.chcnav.com), with a vertical accuracy of 3 cm and a horizontal accuracy of 2 cm, was employed to measure elevations in 2019. Before obtaining the first results, we spent a few minutes to initialize the system. Among the 46 elevation measurements made in total, 33 were located in the flat eastern area, and 13 in the mountainous area (see Fig. 3a). The data were intended to be used to evaluate

Formatted: Font color: Auto

Deleted: The accuracy of ground surface elevation is crucial for groundwater modeling because it influences hydraulic heads, hydraulic gradient, and also groundwater flow and its direction.

Formatted: Font color: Auto

Formatted: Font color: Auto

Deleted: was

seven DEM datasets (Table 2). The most accurate DEM will be applied as the top model boundary in groundwater modeling and also for calculation of hydraulic heads where the ground-based altitude survey is not available. Seven DEMs are all open access and were downloaded from websites of the United States Geological Survey (USGS), Japan Aerospace Exploration Agency (JAXA), and Alaska Satellite Facility (ASF).

Table 2. Seven different DEM datasets.

Number	Name	DEM	Resolution	Source
1	SRTM	Shuttle Radar Topography Mission	1 Arc–Second	USGS
2	ASTER V1	ASTER GDEM Version 1	1 Arc–Second	USGS
3	ASTER V2	ASTER GDEM Version 2	1 Arc–Second	USGS
4	ASTER V3	ASTER GDEM Version 3	1 Arc–Second	USGS
5	AW3D30	ALOS World 3D – 30 m Version 2.2	30 m	JAXA
6	ALOS RT2	ALOS PALSAR RT2	30 m	ASF
7	ALOS RT1	ALOS PALSAR RT1	12.5 m	ASF

3.3 Soil thickness measurement

Due to limited conditions for hydrogeophysical surveys in the mountainous west, we sampled the thickness of the overlying soils in the west to build the hydrogeological conceptual model and to validate simulations of spatially distributed soil thickness by landscape evolution models like LEM LAPSUS (Schoorl et al., 2006; Schoorl et al., 2002) (will be presented in another paper). In the mountainous west, feldspathic quartzose sandstone and sandy slate parent materials show variable soil depths related to landscape position. The fieldwork was carried out at six sites (see Fig. 3b–3g). Measurements in sites 1 and 2 were conducted in 2018, while the rest in 2019. Soil thickness and slope of the ground surface were measured using an auger and a clinometer from Eijkelkamp Soil & Water Company (https://en.eijkelkamp.com). The exact measurement positions at each site were decided based on slope forms and surface pathways.

3.4 Hydrogeological surveys

3.4.1 Water table depth measurement

Water table depth information is important for hydrology and hydrogeology. By subtracting the water table depth from ground surface elevation, a hydraulic head is obtained. A set of hydraulic heads distributed over the study area can be used to determine the regional groundwater piezometric map to enable a general understanding of the groundwater flow system in the study area. We measured 40 water table depths in 34 boreholes during 05-08 August 2018 and 20 August – 05 September 2019 using a dipper (Fig. 3a). In six boreholes, water table depths were measured both in 2018 and 2019. Eight level-loggers were installed to monitor the long–term groundwater level fluctuation, but the data are not available yet.

3.4.2 Aquifer tests

Aquifer tests, including pumping tests and slug tests, were conducted to obtain hydraulic conductivity. The first pumping test was done in 2017, in the borehole ITC_Maqu_1, where core lithology information is available (Fig. 3a). The pumping rate

Formatted: Font color: Auto

Formatted: Font color: Auto

Formatted: Font color: Auto

Deleted: By subtracting the water table depth from ground surface elevation, the hydraulic head and further the regional groundwater piezometric map can be obtained to enable a general understanding of the groundwater flow system in the study area.

Deleted: 36

was constant 55.6 m^3/d measured with a flowmeter, and the pumping duration was about 30 minutes. The pumping rate was limited because the borehole ITC_Maqu_1 could easily collapse if the pumping rate were too high. The water level became stable soon after the start of pumping and was recorded every minute using a data logger (TD–Diver manufactured by Van Essen Instruments, with a range of 10 m). Other tests were carried out in 2019, including two pumping tests and eight slug tests (Fig. 3a). For the two pumping tests with the pumping rate of 31.6 m^3/d and 101.52 m^3/d, due to practical reasons, only water level recovery data were analyzed. In the eight slug tests, the groundwater level was abruptly lowered by extracting 11.75 L water from the well. The water levels were recorded every second or two seconds in slug tests and every five seconds or 20 seconds in pumping tests using a data logger (3001 Levelogger Edge manufactured by Solinst, with a range of 10 m).

The pumping test data acquired from the borehole ITC_Maqu_1 were analyzed using the Boulton (1963) method as follows:

$$S = \frac{Q}{4\pi T} W(U_{AB}, r/D), \quad (1)$$

where S_D is drawdown (m), Q is pumping rate ($m^3.d^{-1}$), T is transmissivity ($m^2.d^{-1}$), $W(U_{AB}, r/D)$ is Boulton's well-function (dimensionless).

Slug tests data were analyzed using the Bouwer and Rice (1976) method for hydraulic conductivity as follows:

$$K = \frac{r^2 \ln\left(\frac{R_e}{R}\right)}{2L} \cdot \frac{1}{t} \cdot \ln\left(\frac{h_0}{h_t}\right), \quad (2)$$

where K is hydraulic conductivity ($m.d^{-1}$), r is the radius of the borehole casing (m), R_e is the effective radial distance over which the head difference is dissipated (m), R is radius measured from borehole center to undisturbed aquifer (m), L is the length of the screen (m), t is time (d), h_0 is the water level at time 0 (m), and h_t is the water level at time t (m).

Another two pumping test data were analyzed using the Boulton and Agarwal method. Agarwal (1980) defines the recovery drawdown S_r (m) as the difference between the head h_p (m) at the end of the pumping period and the head h (m) during the recovery period.

$$S_r = h - h_p \quad (3)$$

The recovery time t_r (d) is the time since the recovery started calculated as the difference between the duration of pumping t_p (d) and the time t (d) since pumping started.

$$t_r = t - t_p \quad (4)$$

3.5 Hydrogeophysical surveys

3.5.1 Magnetic susceptibility

The magnetic susceptibility of rocks changes the local geomagnetic field. The magnetic rocks, which lead to different gradient and intensity of the geomagnetic field, result in different Larmor frequency and further can make the MRS signal undetectable (Lubczynski and Roy, 2007; Plata and Rubio, 2007). The MRS sounding is usually not possible when the magnetic susceptibility is larger than 10^{-2} SI units, but possible when it is lower than 10^{-3} SI units, and may be or may not be possible

Formatted: Font color: Auto

Deleted: The methods used for analyzing the data of pumping tests and slug tests were chosen based on the aquifer information from hydrogeophysical survey and well–related information from local borehole owners.

Formatted ... [1]
Formatted ... [2]
Formatted ... [3]
Formatted ... [4]
Formatted ... [5]
Formatted ... [6]
Formatted ... [7]
Formatted ... [8]
Formatted ... [9]
Formatted ... [10]
Formatted ... [11]
Formatted ... [12]
Formatted ... [13]
Formatted ... [14]
Formatted ... [15]
Formatted ... [16]

within the interval probably depending on the remanent magnetization of the material (Bernard, 2007). Therefore, it is always recommended to measure the magnetic susceptibility before embarking on a large scale MRS survey (Roy et al., 2008). In this study, portable magnetic susceptibility meter SM–20 was used to measure the magnetic susceptibility at 11 sites in the field (Fig. 4). At each site, an average magnetic susceptibility was obtained from 3–5 repeated measurements.

3.5.2 ERT

Subsurface resistivity depends on many different parameters, e.g., lithology, water content, and water conductivity. Its distribution in the subsurface can be visualized by 2D ERT. ERT was employed in this study because it provides subsurface resistivity, which not only supports the analysis of MRS measurements but also can give us a general understanding of the aquifer.

We performed seven ERT surveys with ERT instrument WGMD–9 manufactured by Chongqing Benteng Digital Control Technical Institute (http://www.cqbtsk.com.cn), China using two configurations, Wenner and dipole-dipole. Wenner and dipole-dipole are standard and commonly used configurations. Wenner usually has a good signal–to–noise ratio (S/N) and is good at detecting vertical changes in resistivity, i.e., suitable to image horizontal structures. Dipole-dipole is sensitive to horizontal changes in resistivity, so it is ideal for vertical structure delineation. Multicore cables with a fixed electrode spacing of 10 m were used in the field. The length of cable was 890 m for ERT1 – ERT4, and 810 m for ERT5 – ERT7 (see Fig. 4). Electrode positions were measured with a hand-held GPS instrument Unistrong MG858s (http://www.unistrong.com), with a horizontal and vertical accuracy of 30 cm. The industry–standard RES2DINV V3.54 (Loke, 1999) was employed for ERT inversion.

3.5.3 MRS

MRS was conducted to define aquifer geometry, estimate hydraulic conductivity or transmissivity and water content with depth. In total, 18 soundings (Fig. 4) were performed using MRS instrument Numis Poly, the latest version of MRS equipment from the IRIS Instrument company (http://www.iris–instruments.com). The Larmor frequency, measured with the proton magnetometer in the field, was set at 2241.8 Hz, and the inclination of the earth's magnetic was set at 52° N. A square loop with a side length of 150 m or 100 m was used. Positions were measured with Unistrong MG858s, with a horizontal and vertical accuracy of 30 cm.

To estimate hydraulic conductivity, the decay time constant T_d is used. There are three kinds of T_d: longitudinal decay time constant T_1, transverse decay time constant T_2, and free induction decay time constant T_2^*. With the current instrument, only T_1 (actually an approximate value T_1^*) and T_2^* are available. The Seevers equation (Seevers, 1966) (Eq. 5) and the Kenyon equation (Kenyon et al., 1989) (Eq. 6) can be used for estimating hydraulic conductivity K (m/d):

$$K = C_p \theta_{MRS} T_d^2 \quad (5)$$

$$K = C_p \theta_{MRS}^4 T_d^2 \quad (6)$$

Formatted: Font color: Auto
Formatted: Font color: Auto
Formatted: Font color: Auto
Formatted: Font color: Auto
Formatted: Font color: Auto
Formatted: Font color: Auto
Deleted: 1
Deleted: 2
Deleted: 1
Deleted: 2

where C_p is the calibration coefficient, which is a lithology dependent factor that needs to be calibrated from the pumping test (dimensionless). θ_{MRS} is the MRS estimated water content (%). Compared to the Kenyon equation, Seevers equation is more accurate (Plata and Rubio, 2008) and has been widely used (e.g., Legchenko et al. (2002), Vouillamoz et al. (2007), Nielsen et al. (2011)) and is used in this study. Once K is estimated, the transmissivity T (m^2/d) can be calculated using the equation:

$$T = K \cdot \Delta z \quad (7)$$

where Δz is the layer thickness (m) derived from MRS inversion.

Based on the study from Vouillamoz et al. (2008), MRS transmissivities are close to transmissivities estimated from pumping tests, the uncertainties in transmissivity estimated from MRS and pumping tests are comparable, and the mean relative uncertainty of the MRS determined water content is 20%. Boucher et al. (2009) and Vouillamoz et al. (2014) confirmed that aquifer transmissivity could be estimated from MRS results with an averaged uncertainty of about 70%.

MRS data were interpreted with an open-access software Samovar V6.6 from the IRIS Instrument company (http://www.iris–instruments.com), which is based on the Tikhonov regularization method (Legchenko and Shushakov, 1998). Samovar assumes the default calibration coefficient C_p of 7E–09 for sandy aquifers and aquifers composed of weathered and highly fractured rock based on MRS calibration experience in France (Legchenko et al., 2004). In this study, C_p was estimated using pumping test data.

3.5.4 TEM

Compared to ERT, TEM also provides subsurface resistivity but with deeper penetration, a relatively lower resolution, and a shorter time of data acquisition. TEM instrument is usually operated in a 1D sounding mode as compared to the ERT 2D profiling mode. Since magnetic fields propagate faster in resistive media than in conductive ones, TEM is advantaged in low resistivity media and mapping deep conductive targets. Similarly to MRS but with different constraints, there is a dead time between the excitation or transmitter function and the detection or receiver function which are time-shared. Such TEM deadtime is much shorter than in the case of MRS. TEM commonly involves placing a square loop on the targeted place and performing soundings. It generates a primary magnetic field that is abruptly interrupted to produce induced eddy currents in the subsurface. The eddy currents will lead to a secondary magnetic field, which can be detected by the loop on the ground surface. The received signals can be used to estimate subsurface resistivities by using appropriate inversion techniques (Nabighian and Macnae, 1991).

The TEM soundings were performed at ten locations (Fig. 4) using TEM instrument TEM–FAST 48. Developed by Applied Electromagnetic Research Limited (http://www.aemr.net), TEM–FAST 48 is very small, compact, portable, and easy to deploy and apply in the field (Gonçalves, 2012). Only one TEM configuration was used, i.e., coincident square loop, of one loop that combines functions of the transmitter and receiver. At each location, different loop sizes (3 m – 95 m), time ranges (3 – 9), stacks (5 – 10), and currents (0.7 A – 1.1 A) were applied to select the optimal data set, which has the maximum investigation depth. If abrupt changes occurred in the obtained curve, presenting the relation between apparent specific resistivity and time,

Deleted: 3

Formatted: Font color: Auto

Formatted: Font color: Auto

Formatted: Font color: Auto

Formatted: Font color: Auto

the measurement was repeated to ensure data quality. After field collection, data were processed using TEM–Researcher proprietary software (http://www.aemr.net) based on the solution of the inverse problem in time domain electromagnetic sounding.

4 Results and Discussion

4.1 Borehole core lithology

The core lithology of the borehole ITC_Maqu_1 is shown in Table 3, Fig.5a, and Fig.5b. The top layer is eolian sand and loam. There are dunes that have been blown out of the river bed on top of the terraces. The deep layer is fluvial sediment. Based on the lithology information, the range of lithology related parameters can be estimated. According to Chen et al. (1999), the Ruoergai Basin was occupied by a large inland lake during the Quaternary before around 40 ka BP, while currently, it is a dry lake basin, with lake deposits exceeding 300 m in thickness. The extend of the ancient lake and Quaternary lake deposits are shown in Fig. 5c. Based on Fig. 5c and the log of the ITC_Maqu_1 borehole shown in Table 3 and Fig.5a, the east of our study area is covered with thick lake sediments at depth, while the shallower part is covered with the Yellow River deposits with the thickness larger than 32 m. This conclusion is consistent with the log of two other boreholes located to the east of the study area in Ruoergai Basin, RM (33°57′, 102°21′) and RH (33°54′, 102°33′) (Fig. 5). RH is about 40 km east of the study area, with a depth of 120 m, not reaching bedrock. The top 12.4 m of coarse sediment, i.e., sands, was deposited by rivers, while the deeper deposits are lake sediments, mainly composed of silt clay, clay silt, and clay (Wang et al., 1995). RM is about 20 km east of the study area, with a depth of 310 m. Like RH, RM core also reveals thick lake sediments, with thin river deposits on the top (Xue et al., 1998).

Table 3. The core lithology of the borehole ITC_Maqu_1.

Depth (m)	Thickness (m)	Lithology
0.0 ~ 0.8	0.8	sandy loam
0.8 ~ 25.5	24.7	fine sand
25.5 ~32.0	6.5	fine sand with gravel

Formatted: Font color: Auto
Formatted: Font color: Auto
Formatted: Font color: Auto
Formatted: Font color: Auto
Deleted: The lithology is shown in Table 3.
Formatted: Font color: Auto
Deleted: would be

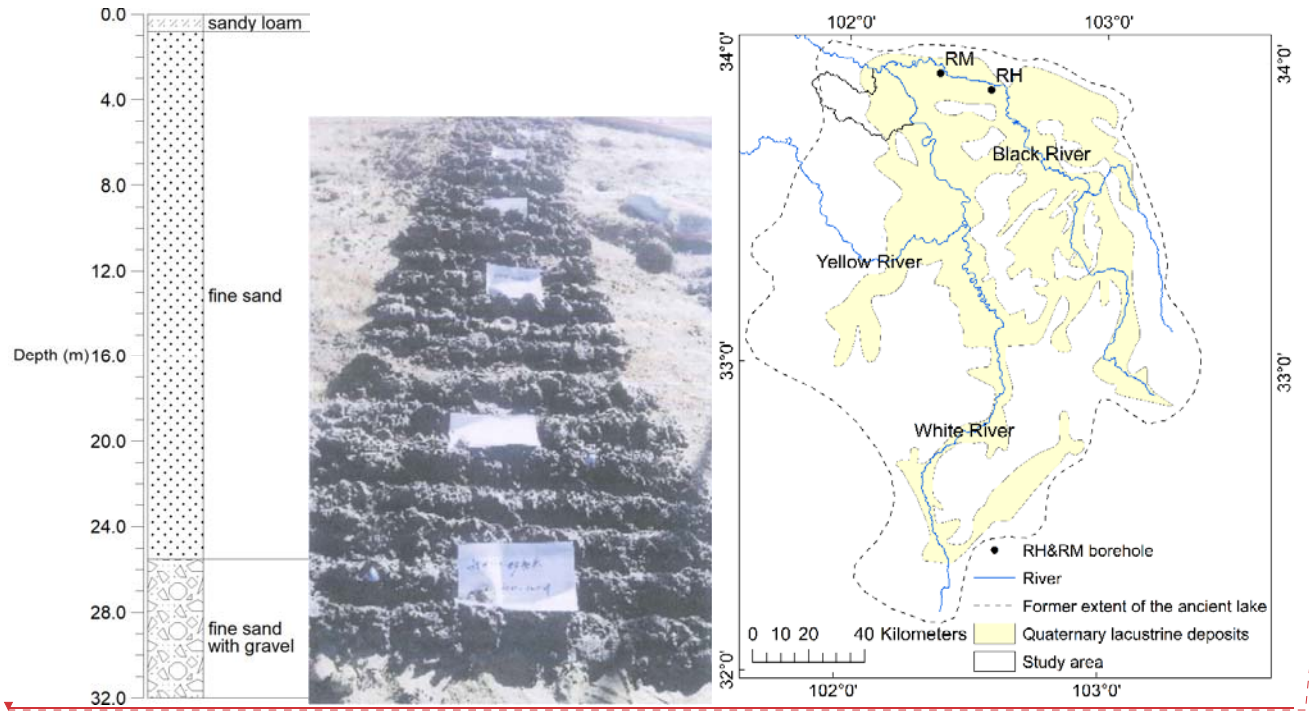

Figure 5. Borehole information: (a) The core lithology of borehole ITC_Maqu_1; (b) A picture of the core sediment when the borehole was drilled; (c) Location of boreholes RM and RH (after Chen et al. (1999)).

4.2 Altitude survey

46 elevations were measured, 33 in the flat east, 13 in the mountainous west, and were used to evaluate the accuracies of seven DEM datasets (Fig. 6) and select the most accurate one. The statistical analysis results of the seven DEMs in the study area are shown in Table 4. The root mean squared error (RMSE) of ALOS RT1 and ALOS RT2 are 5.695 m and 5.477 m, respectively, much smaller than the RMSE of the other five DEMs. The correlation coefficient, the mean error, and the mean absolute errors of ALOS RT1 and ALOS RT2 also show better performance than those of the other five DEMs. Comparing ALOS RT1 with ALOS RT2, ALOS RT1 slightly outperforms ALOS RT2 with regards to RMSE, correlation coefficient, and the mean error. Table A1 and Table A2 in the Appendix list the statistical analysis results of seven DEMs, separately for the flat eastern area and the mountainous western area. Seven DEMs all behave better in the west than the east in terms of the correlation coefficient. In the west, the correlation coefficients of seven DEMs are all larger than 0.94, while in the east, the correlation coefficients are all lower than 0.24. This is because the range of elevation in the flat east is much smaller than the range of elevation in the mountainous west. With regard to the RMSE, mean error, and mean absolute error, all seven DEMs have better behavior in the east than in the west. In general, ALOS RT1 and ALOS RT2 also outperform the other five DEMs, according to Table A1 and Table A2.

Deleted:

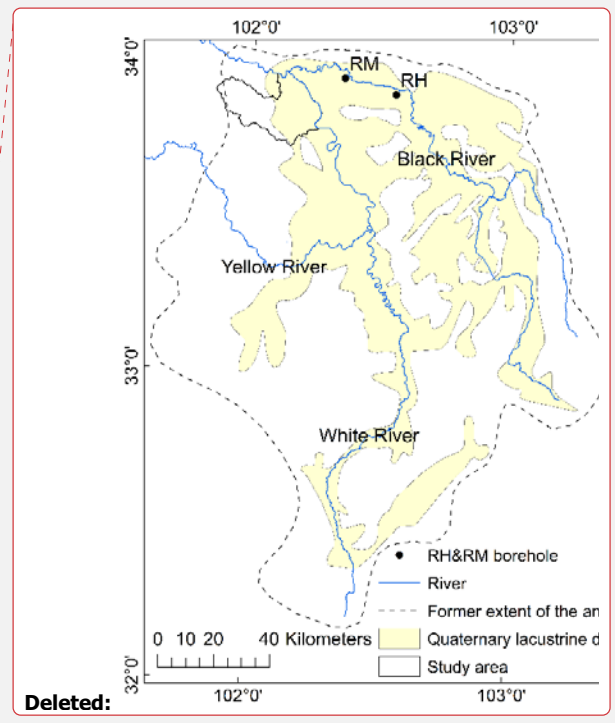

Formatted: Font color: Auto

Formatted: Font color: Auto

Formatted: Font color: Auto

Deleted: Figure 5. Location of boreholes RM and RH (after Chen et al. (1999)).¶

Since ALOS RT1 performs slightly better than ALOS RT2 in the whole study area and has a higher resolution than ALOS RT2, it is the most suitable DEM to use in this study area. For ALOS RT1 in the flat east, 52% errors (DEM value – GPS-RTK value) are within the range of –3 m to 3 m, and 79% errors are within the scope of –5 m to 5 m. While in the mountainous west, 54% errors are within the range of –8 m to –12 m, and 46% errors are within the range of 0 m to 7 m.

Previous TP works about DEM evaluation mainly focused on SRTM and ASTER. Our results are generally consistent with previous studies in terms of RMSE of SRTM. Nan et al. (2015) evaluated the height accuracy of SRTM and ASTER in eastern TP with reference to the relatively high precision of 1:50,000 scale DEM surveyed and mapped by the State Bureau of Surveying and Mapping in China. As a result, RMSE of SRTM and ASTER are 35.3 m and 50.2 m, respectively. Ye et al. (2011) evaluated SRTM and ASTER in the Mt. Qomolangma (Mt. Everest) area on the TP, by comparing 211 elevation checkpoints on the 1:50,000 topographic maps surveyed and mapped by State Bureau of Surveying and Mapping in China, demonstrating an average height difference of 31.3 m and 44.9 m for SRTM and ASTER, respectively. However, there are other studies that have different evaluation results. Fujita et al. (2008) found that the elevation differences between DEMs and ground survey data from differential GPS were 11.0 m for ASTER and 11.3 m for SRTM in the Lunana region, Bhutan Himalaya. The DEM evaluation results also indicated that in different places over the TP, the satellite DEM estimates are acquired with varying accuracy. This may be due to different topographic complexity in different areas.

The DEMs' quality can be influenced by several factors, such as sensor type, algorithm, terrain type, and grid spacing. (Hebeler and Purves, 2009). In this study, grid spacings of DEMs are similar except for ALOS RT1, so the main factors that affect the accuracy of the DEMs should be sensor types and algorithms. For SRTM, the issue inherent to the production method is mast oscillations, while for ASTER and AW3D30, the issue is scene mismatch (Grohmann, 2018). As for radiometrically terrain corrected (RTC) products ALOS RT1 and ALOS RT2, the quality is directly related to the quality of the source DEM SRTM which was used in the RTC process. This results in very similar correlation coefficients of SRTM, ALOS RT1, and ALOS RT2, and obvious improvements in RMSE, MAE, and ME (Table 4).

Formatted: Font color: Auto
Formatted: Font color: Auto
Formatted: Font color: Auto
Formatted: Font color: Auto
Formatted: Font color: Auto

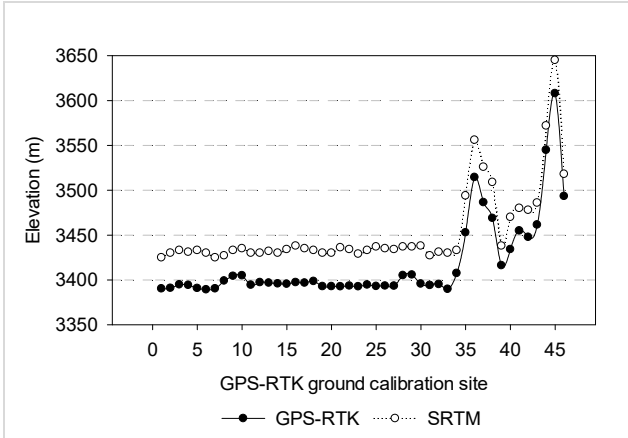

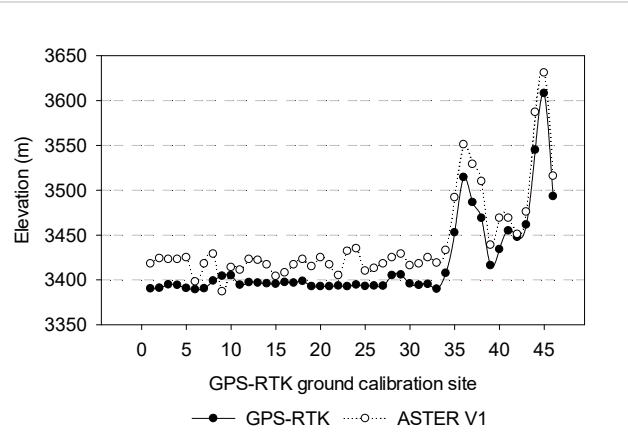

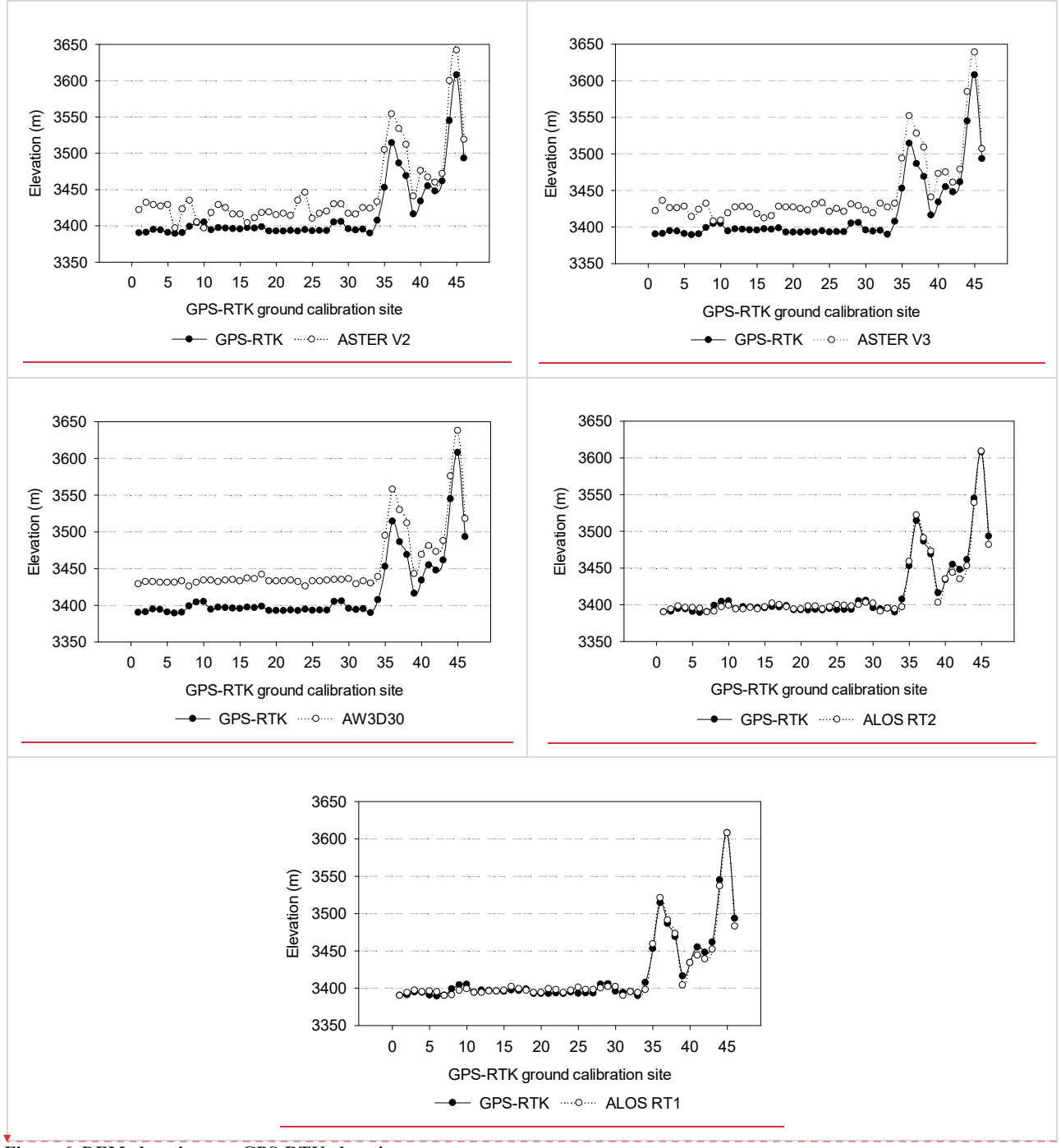

Figure 6. DEM elevations vs. GPS-RTK elevations.

Deleted:

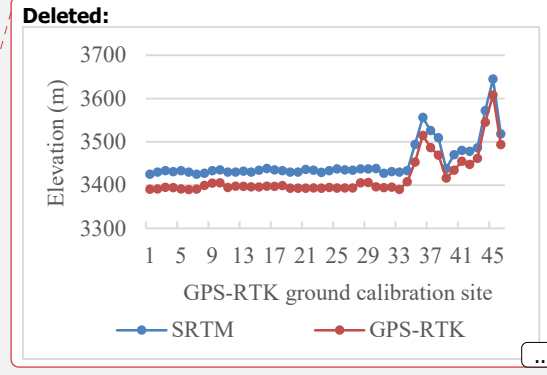

... [17]

Table 4. Statistical analysis of seven DEMs in the study area.

DEM	Resolution	Min Error * (m)	Max Error (m)	Max Error – Min Error (m)	MAE (Mean Absolute Error) (m)	ME (Mean Error) (m)	Correlation coefficient	RMSE (m)
SRTM	1 Arc–Second	22	44	22	35.488	35.488	0.985	35.936
ASTER V1	1 Arc–Second	–17	43	60	24.761	24.010	0.950	26.565
ASTER V2	1 Arc–Second	–8	55	63	27.483	27.140	0.941	30.171
ASTER V3	1 Arc–Second	4	45	41	28.988	28.988	0.962	30.438
AW3D30	30 m	25	44	19	36.249	36.249	0.985	36.707
ALOS RT2	30 m	–13	8	21	4.592	–0.338	0.985	5.695
ALOS RT1	12.5 m	–12	8	20	4.404	–0.360	0.986	5.477

* Error = DEM value – GPS-RTK value

4.3 Soil thickness measurement

Results of soil thickness measurements are listed in Table 5 (location shown in Fig.3). The soil thickness decreases as the slope increases, and are within 1.2 m in most cases (Fig. 7). Under the soil layer, a less weathered layer exists where water can also flow and needs to be taken into account in the conceptual model. In the field, the difference between the less weathered layer and the soil layer is that the less weathered layer contains partially weathered stones. According to the owners of three wells located in or near the valley, the depths of three wells are larger than 10 m and do not reach bedrock. Studies from Yan et al. (2020) and Shangguan et al. (2017) estimated the depth to bedrock within China and on a global scale, respectively. By combining the depth to bedrock information with our results, the thickness of the less weathered layer can be estimated later when establishing the hydrogeological conceptual model.

Table 5. Soil thickness measurements, locations of each measurement can be found in Figure 3.

No.	Depth (cm)	Slope (°)	Elevation* (m)	No.	Depth (cm)	Slope (°)	Elevation* (m)	No.	Depth (cm)	Slope (°)	Elevation* (m)
1	39	9	3762	27	71	10	3509	53	102	6	3457
2	45	20	3769	28	90	11	3503	54	102	14	3459
3	28	25	3777	29	>120	5	3493	55	104	6	3460
4	48	16	3784	30	110	5	3488	56	100	13	3462
5	50	22	3783	31	>120	5	3482	57	92	10	3469
6	46	14	3775	32	>107	2	3473	60	40	9	3491
7	39	25	3770	33	>110	4	3479	61	53	6	3480
8	34	41	3757	34	59	13	3488	62	61	15	3478
9	37	22	3750	35	85	13	3491	63	70	7	3476
10	42	19.5	3734	36	60	20	3502	64	63	14	3468
11	23	20	3732	37	92	13	3517	65	61	9	3467
12	52	0	3461	38	38	10	3452	66	87	10	3458
13	42	3	3462	39	41	20	3461	67	60	5	3496
14	35	3	3463	40	76	30	3472	68	63	7	3487

Formatted ... [18]
Deleted: Soil thickness measurements (Table 5) indicate th ... [19]
Formatted ... [20]
Deleted: No. ... [21]
Formatted ... [22]
Formatted ... [23]
Formatted ... [24]
Formatted ... [25]
Formatted ... [26]
Formatted ... [27]
Formatted ... [28]
Formatted ... [29]
Formatted ... [30]
Formatted ... [31]
Formatted ... [32]
Formatted ... [33]
Formatted ... [34]
Formatted ... [35]
Formatted ... [36]
Formatted ... [37]
Formatted ... [38]
Formatted ... [39]
Formatted ... [40]
Formatted ... [41]
Formatted ... [42]
Formatted ... [43]
Formatted ... [44]
Formatted ... [45]
Formatted ... [46]
Formatted ... [47]
Formatted ... [48]
Formatted ... [49]
Formatted ... [50]
Formatted ... [51]
Formatted ... [52]
Formatted ... [53]
Formatted ... [54]
Formatted ... [55]
Formatted ... [56]
Formatted ... [57]
Formatted ... [58]
Formatted ... [59]
Formatted ... [60]
Formatted ... [61]
Formatted ... [62]
Formatted ... [63]
Formatted ... [64]
Formatted ... [65]
Formatted ... [66]

15	38	4	3470	41	55	30	3483	69	68	15	3474
16	50	9	3474	42	32	40	3501	70	87	18	3554
17	40	10	3482	43	80	35	3519	71	30	14	3562
18	38	10	3489	44	27	30	3530	72	85	20	3572
19	42	15	3502	45	49	30	3522	73	41	17	3587
20	37	8	3494	46	52	30	3514	74	83	13	3596
21	40	10	3488	47	43	20	3500	75	67	27	3612
22	30	5	3475	48	44	22	3484	76	63	20	3605
23	30	4	3472	49	30	25	3475	77	>110	20	3593
24	35	4	3469	50	74	14	3470	78	>110	10	3574
25	28	1	3463	51	37	12	3464	79	42	15	3564
26	29	0	3459	52	81	6	3447				

*Elevations were extracted from ALOS PALSAR RT1.

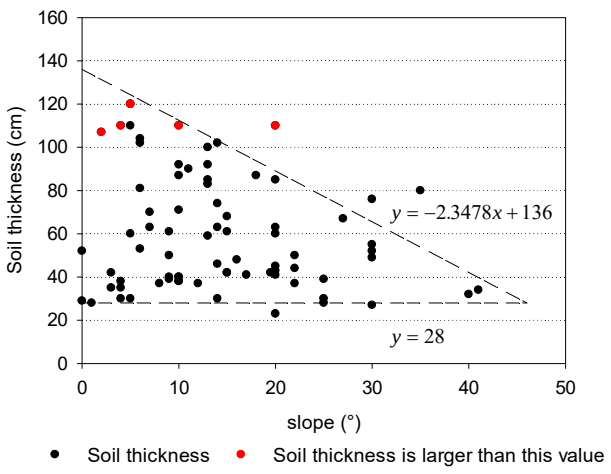

Figure 7. Soil thickness (m) vs. slope (°).

4.4 Hydrogeological surveys

4.4.1 Water table depth measurement

22 water table depths were measured in 2018, and 18 water table depths were measured in 2019 (Table 6). In the flat eastern area, the depths were interpolated in Surfer using the default Ordinary Kriging method with the linear variogram model (slope=1, anisotropy ratio=1, anisotropy angle=0) which provides reasonable grids in most circumstances (Fig. 8a and Fig. 8b). Owing to the fact that most people living in the mountainous west use water from streams, so only three boreholes were found and water table depths were measured in the west. Three measurements are far from enough to provide a reasonable estimation of water table depth in the west, so they were excluded during interpolation. In both 2018 and 2019, the interpolated water table depths show a similar trend that the depth increases from the middle of the study area to the eastern boundary. However, the range of water table depth in 2018 is slightly larger than the range of water table depth in 2019. This is because

Formatted ... [67]
Formatted ... [68]
Formatted ... [69]
Formatted ... [70]
Formatted ... [71]
Formatted ... [72]
Formatted ... [73]
Formatted ... [74]
Formatted ... [75]
Formatted ... [76]
Formatted ... [77]
Formatted ... [78]
Formatted ... [79]
Formatted ... [80]
Formatted ... [81]
Formatted ... [82]
Formatted ... [83]
Formatted ... [84]
Formatted ... [85]
Formatted ... [86]
Formatted ... [87]
Formatted ... [88]
Formatted ... [89]
Formatted ... [90]
Formatted ... [91]
Formatted ... [92]
Formatted ... [93]
Formatted ... [94]
Formatted ... [95]
Formatted ... [96]
Formatted ... [97]
Formatted ... [98]
Formatted ... [99]
Formatted ... [100]
Formatted ... [101]
Formatted ... [102]
Formatted ... [103]

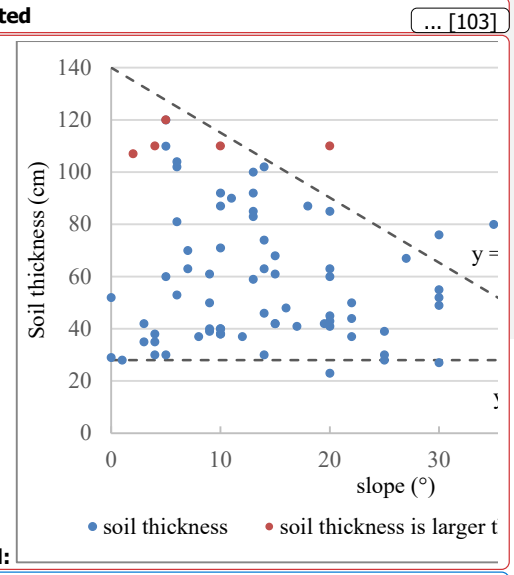

Deleted:
Field Code Changed ... [104]
Formatted ... [105]
Deleted: Owing to the fact that most people living in the ... [106]

the dam gates were open to lower the water level in the reservoir (Fig. 3a) in 2019 to facilitate nearby constructions. So water table depths at positions 1, 11, 21, and 22 were smaller in 2019 compared to 2018 (see Fig. 8a and Fig. 8b). In general, the range of water table depth is between 0.0 m to 19.1 m in 2018 and between 0.7 m to 18.0 m in 2019.

Among 36 boreholes, elevations measured by GPS-RTK are only available for 13 boreholes, and they are shown in Table 7 with two decimal places. ALOS RT1 extracted elevations are in integer form due to relatively low accuracy. These elevations are used to derive hydraulic heads by subtracting the water table depths from the ground surface elevation. Using the Kriging method, hydraulic heads were interpolated to obtain piezometric maps in the flat east (Fig. 8c and Fig. 8d). According to the map, in both 2018 and 2019, hydraulic heads decrease from the middle of the study area to the eastern boundary. The difference of water table depth in 2018 and 2019 (Fig. 8c) is mainly caused by 1) different positions and amount of control points; 2) the gates were open to lower the water level in the reservoir in 2019;

In the study area, the western part plays a vital role in collecting water, whereas the eastern is mainly for storing water. Streams flow from the mountainous west to the flat east, and also, groundwater flows from west to east, recharging the Yellow River. This is consistent with the conclusion from Chang (2009) that the groundwater in Maqu county is recharging the Yellow River.

Table 6. Water table depth measurements. GPS-RTK measurements of elevations are given with two decimal places, while ALOS RT1 extracted ones given in integer form.

Borehole	Latitude (°)	Longitude (°)	Elevation (m)	Logger installed date (dd/mm/yy)	2018 Measurement			2019 Measurement		
					Date (dd/mm)	Depth (m)	Head (m)	Date (dd/mm)	Depth (m)	Head (m)
1	33.932	102.117	3401		05/08 – 08/08	18.80	3382	24/08	17.95	3383
2	33.921	102.149	3395		05/08 – 08/08	13.22	3382			
3	33.918	102.136	3394		05/08 – 08/08	13.65	3380			
4	33.904	102.127	3396		05/08 – 08/08	8.40	3388			
5	33.890	102.128	3395		05/08 – 08/08	1.20	3394			
6	33.876	102.093	3406		05/08 – 08/08	2.50	3404	23/08	2.40	3404
7	33.864	102.126	3393		05/08 – 08/08	0.68	3392			
8	33.864	102.146	3398		05/08 – 08/08	2.00	3396			
9	33.863	102.147	3394		05/08 – 08/08	1.96	3392			
10	33.877	102.172	3397		05/08 – 08/08	9.13	3388			
11	33.884	102.198	3390.25		05/08 – 08/08	9.90	3380.35	27/08	9.50	3380.75
12	33.860	102.190	3393		05/08 – 08/08	10.02	3383			
13	33.857	102.170	3395		05/08 – 08/08	6.30	3389			
14	33.837	102.141	3394		05/08 – 08/08	1.37	3393			
15	33.811	102.143	3401		05/08 – 08/08	0.80	3400			

Formatted: Font color: Auto

Deleted: At 13 water table depth measurement locations, the elevations are available from the GPS-RTK survey and are shown in Table 7 with two decimal places, while

16	33.790	102.147	3405.67	29/08/2019	05/08 – 08/08	1.47	3404.20	29/08	1.48	3404.19
17	33.832	102.189	3396		05/08 – 08/08	8.57	3387			
18	33.824	102.185	3395		05/08 – 08/08	7.08	3388			
19	33.820	102.185	3398		05/08 – 08/08	7.72	3390			
20	33.818	102.186	3401		05/08 – 08/08	6.77	3394			
21	33.830	102.225	3392.64	28/08/2019	05/08 – 08/08	12.80	3379.84	28/08	12.08	3380.56
22	33.794	102.214	3395.64		05/08 – 08/08	10.51	3385.13	29/08	9.75	3385.89
23	33.947	102.135	3398.92	27/08/2019				27/08	11.16	3387.76
24	33.916	102.155	3394.00					04/09	11.70	3382.30
25	33.872	102.143	3394.41					23/08	2.23	3392.18
26	33.865	102.132	3395.15	05/09/2019				05/09	1.63	3393.52
27	33.860	102.194	3394.10	28/08/2019				28/08	9.30	3384.80
28	33.774	102.187	3400					20/08	4.10	3396
29	33.776	102.168	3405.03					20/08	1.20	3403.83
30	33.794	102.129	3401					20/08	1.20	3400
31	33.815	102.117	3400					20/08	0.65	3399
32	33.817	102.080	3454.88	01/09/2019				01/09	3.60	3451.28
33	33.866	101.983	3461.53	03/09/2019				03/09	1.70	3459.83
34	33.884	101.927	3514.40	31/08/2019				31/08	4.74	3509.66

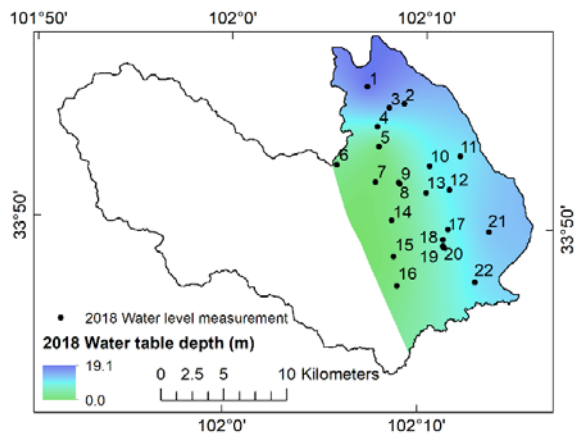

(a) (made during 05-08 August 2018)

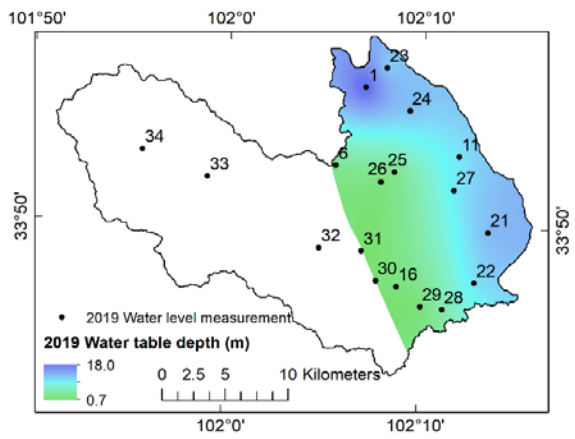

(b) (made during 20 August – 05 September 2019)

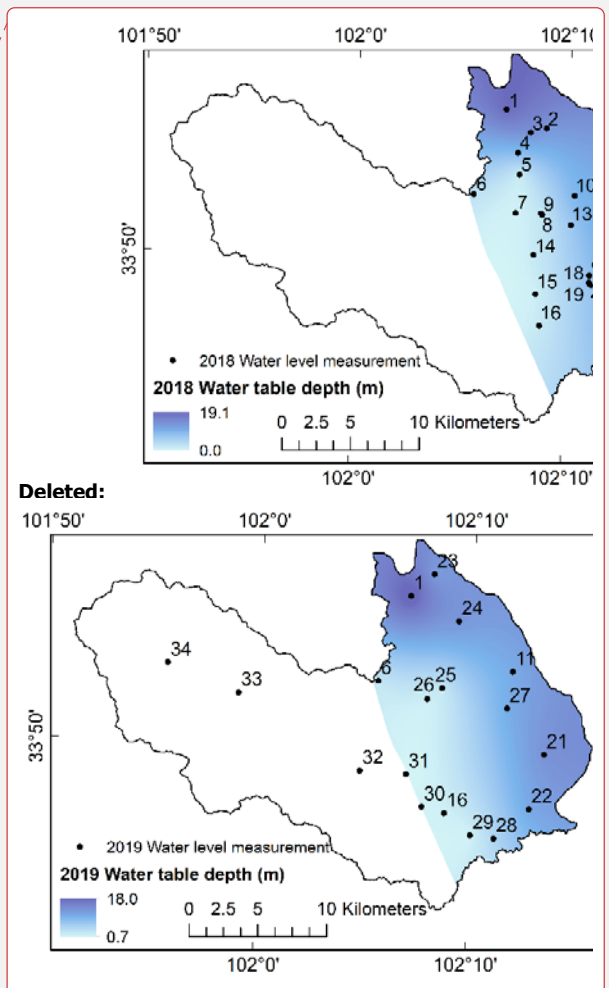

(a)

... [107]

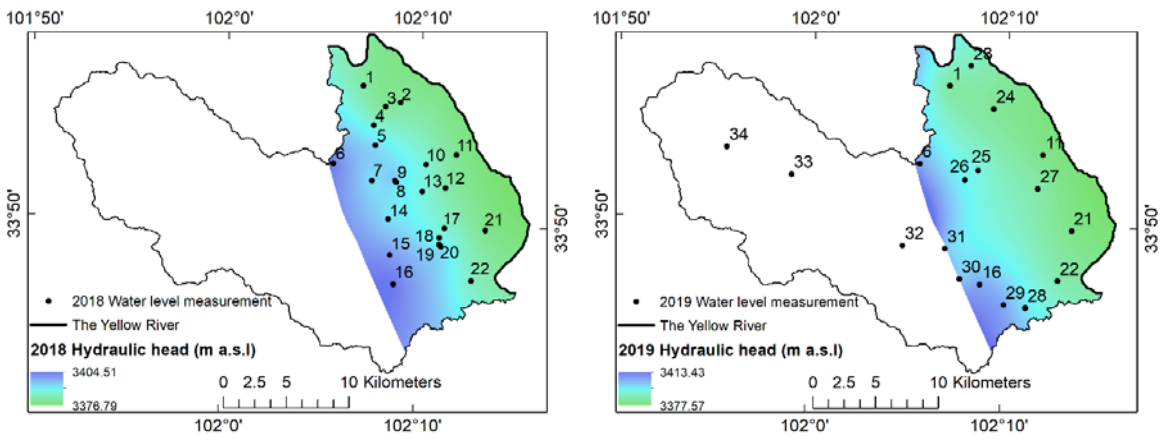

(c) (made during 05-08 August 2018) (d) (made during 20 August – 05 September 2019)

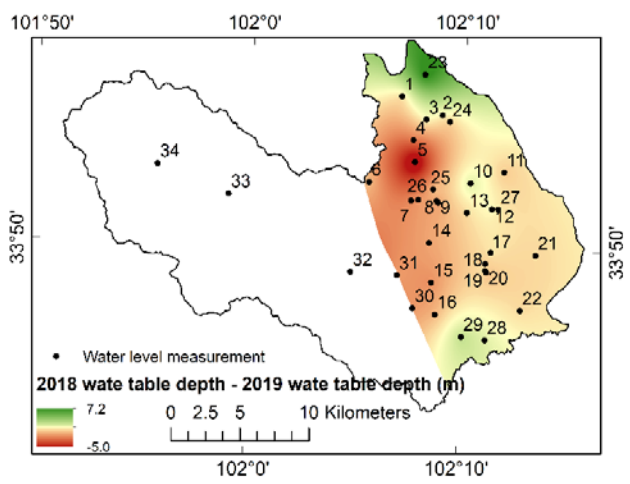

(e)

Figure 8. Water table depths (m) and piezometric heads (m a.s.l) of east Maqu catchment. (a) and (b) are water table depths (m) of east Maqu catchment in 2018 and 2019, respectively; (c) and (d) are piezometric heads (m a.s.l) of eastern Maqu catchment in 2018 and 2019, respectively; (e) is the difference (m) of water table depth between 2018 and 2019. Numbers from 1 to 34 are identification numbers of boreholes listed in Table 6.

4.4.2 Aquifer tests

11 aquifer tests were conducted (Fig. 9, Fig. 3a) in unconfined aquifers, in partially penetrating boreholes. Eight slug tests were done in boreholes numbered 16, 21, 24, 26, 27, 32, 33, 34 (Fig. 8), two pumping tests were carried out in 2019 were at boreholes 6 and 23 (Fig. 8), and one pumping test was carried out in 2017 at the borehole ITC_Maqu_1. Data were processed automatically in AquiferTest software with assumptions made considering the average conditions in the study area: aquifer is unconfined and 35 m thick; well is partially penetrating; screen radius is 0.27 m; screen length is 15 m; the distance from aquifer top to screen bottom is 15 m; casing radius is 0.25 m; borehole radius is 0.3 m. As a result, the hydraulic conductivities

Formatted: Justified

Formatted: Font color: Auto

Deleted: **Figure 8. (a) and (b) are water table depths (m) of east Maqu catchment in 2018 and 2019, respectively; (c) and (d) are piezometric heads (m a.s.l) of eastern Maqu catchment in 2018 and 2019, respectively; (e) is the difference (m) of water table depth between 2018 and 2019. Numbers from 1 to 34 indicate boreholes listed in Table 6.¶**

Formatted: Font color: Auto

Deleted: 11 aquifer tests were conducted (Fig. 9) in unconfined aquifers, where the wells are partially penetrating. The pumping test data acquired from the borehole ITC_Maqu_1 were analyzed using the Boulton (1963) method as follows: ¶

$S_D = \frac{2\pi T(H-b)}{Q}$,

where S_D is drawdown (m), T is transmissivity (m^2/d), H is the average head along the saturated thickness (m), b is the original saturated aquifer thickness (m), and Q is pumping rate (m^3/d).¶

Eight slug tests were done in boreholes numbered 16, 21, 24, 26, 27, 32, 33, 34 (Fig. 8) and the data were analyzed using the Bouwer and Rice (1976) method for hydraulic conductivity as follows: ¶

$K = \frac{r^2 \ln\left(\frac{R_e}{R}\right)}{2L} \cdot \frac{1}{t} \cdot \ln\left(\frac{h_0}{h_t}\right)$,

where K is hydraulic conductivity (m/d), r is the radius of the well casing (m), R_e is the effective radial distance over which the head difference is dissipated (m), R is radius measured from well center to undisturbed aquifer (m), L is the length of the screen (m), t is time (d), h_0 is the water level at time 0 (m), and h_t is the water level at time t (m). ¶

Another two pumping tests were carried out at borehole 6 and 23. The water level recovery data were analyzed using the Boulton and Agarwal method. Agarwal (1980) defines the recovery drawdown S_r (m) as the difference between the head h_p (m) at the end of the pumping period and the head h (m) during the recovery period. ¶

$S_r = h - h_p$,

The recovery time t_r (d) is the time since the recovery started calculated as the difference between the duration of pumping t_p (d) and the time t (d) since pumping started. ¶

$t_r = t - t_p$,

range from 0.1 m/d to 15.6 m/d (Fig. 9 and Fig. A1), which according to Healy et al. (2007), can be classified as hydraulic conductivity of fine silty sand to coarse clean sand. However, the slug test in borehole 24 provided lower estimates of hydraulic conductivity than the nearby pumping test in borehole ITC_Maqu_1, which likely underestimated the hydraulic conductivity as borehole 24 was not used for a period of time. Therefore, compared to the slug test, the hydraulic conductivity obtained from the pumping test is more accurate and is a volumetric average, which makes it more suitable to calibrate C_p, because MRS results are also volumetric averages.

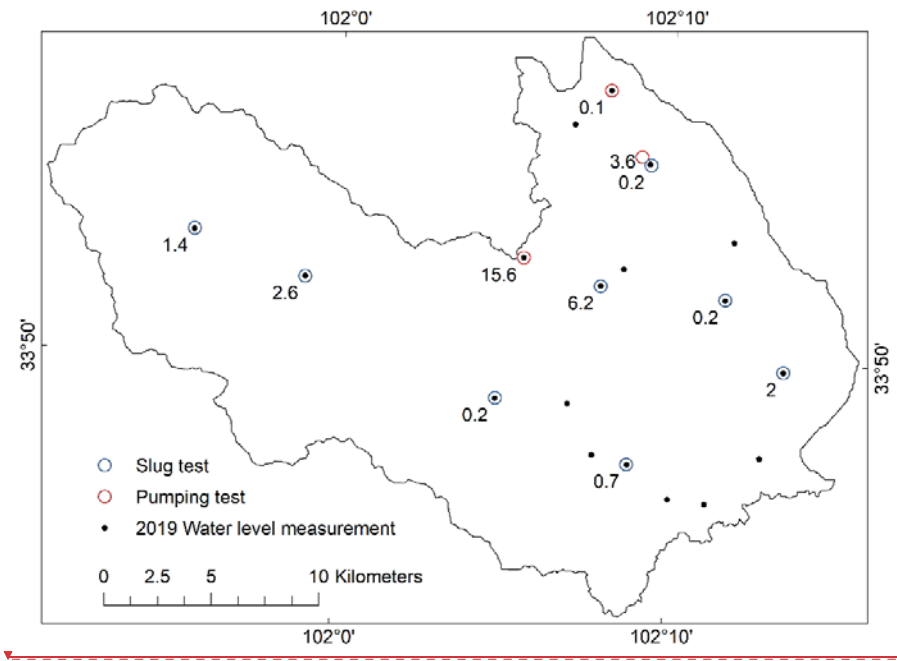

Figure 9. Hydraulic conductivity (m.d^{-1}) obtained from aquifer tests, east of Maqu catchment.

4.5 Hydrogeophysical surveys

4.5.1 Magnetic susceptibility

The magnetic susceptibility measurements (Fig. 10) reveal very low susceptibility in the catchment with susceptibility values, all smaller than 1×10^{-5} SI units with an average of 3×10^{-6} SI units. A previous study from Chen et al. (1999) also reported low magnetic susceptibility of the RH core (Fig. 5) with 120 m length located 40 km east of the study area in Ruoergai Basin. Thus, the low magnetic susceptibility ensured the suitability of applying MRS in the study area.

Formatted: Font color: Auto

Formatted: Font color: Auto

Formatted: Font color: Auto

Formatted: Font color: Auto

Deleted: . According to Healy et al. (2007), the hydraulic conductivity is roughly between 0.1 m/d - 100 m/d when the earth material changes from fine silty sand to coarse clean sand. So the obtained hydraulic conductivities are acceptable. However, the slug test is likely to underestimate the hydraulic conductivity when the well is not used for a period of time. Compared

Deleted:

Formatted: Font color: Auto

Deleted: Figure 9. Hydraulic conductivity (m/d) obtained from aquifer tests, east of Maqu catchment.¶

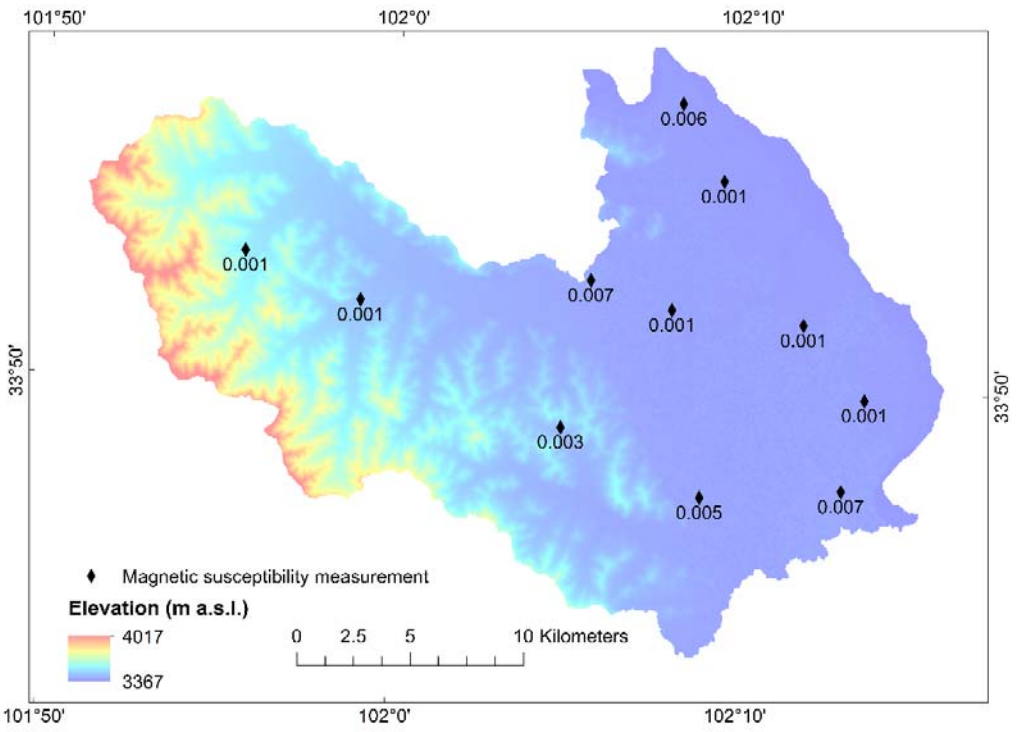

Figure 10. Magnetic susceptibility measurements (10^{-3} SI Units) ensured the suitability of applying MRS in the study area.

4.5.2 ERT

Detailed information on ERT profiles and inversion parameters are listed in Table 7 and Table A3, respectively. The pseudosection plot in RES2DINV is useful for filtering out outlier data points, after which the least square method was used for the inversion. Results of ERT2 and ERT3 are shown in Fig. 11, and complete results are shown in Fig. A2 in the Appendix, with the root mean square (RMS) error less than 5%. A pattern of roughly regular parallel to surface electrostratigraphy is observed in all ERT profiles, except 0 m – 310 m of profile ERT5, where the pattern is dipping relatively to surface. This means that strata are likely to be stratified in most parts of the study area. For ERT2, ERT3, ERT5, and ERT6, three electrostratigraphic layers can be identified: the first layer with the highest resistivity, the second layer with the lowest resistivity, and the third layer with a medium resistivity. The second layer is likely to represent an aquifer. However, considering ERT4 and ERT7, there is a lack of marker electrostratum, i.e., a layer with high resistivity does not exist at the ground surface. This is probably due to high water content near the ground surface in the mountainous area where ERT4 and ERT7 were located. As for ERT1, rainfall occurred during the field measurement. Rainwater accumulations occurred next to some of the electrodes, causing abnormal current distribution during the ERT measurements and about half of the data are missing in the filtering process. The ERT1 inversion results show a three – layers pattern similar to the one observed along the ERT2, ERT3, ERT5, and ERT6 profiles. One or more short wavelength anomalies (< 200 m) are observed along all profiles

but particularly in the case of ERT1, ERT3 and ERT6. Short wavelength anomalies along ERT1 may be due to data acquisition made during rainfall, while in the case of the other profiles, localized changes in water content or lithology variations are suspected.

Compared to the Dipole-Dipole configuration, the investigation depth of the Wenner configuration is deeper. So resistivity values obtained from Wenner configuration were used to establish geoelectrical models for MRS inversion. For ERT2, ERT3, ERT5, and ERT6, three-layer geoelectrical models were extracted, while for ERT4 and ERT7, two-layer geoelectrical models were extracted. ERT1 was neglected due to the influence of rainfall. For ERT5, from 0 m to 310 m, there's a topographic change, the ground surface elevation decreases from 3395 m.a.s.l and stabilizes at around 3390 m.a.s.l. Ground surface with low resistivity exists along this 310 m transect. Since the MRS soundings were conducted in flat areas, so only resistivity from 310 m to 810 m was used for the first layer of the geoelectrical model. The geoelectrical models and corresponding MRS measurements are shown in Table A4. The depths of the last layer of geoelectrical models are extended to 1.5 times of the MRS investigation depth since signal distortion due to subsurface resistivity is calculated down to that depth while making the MRS linear filter. In this particular version, MRS investigation depth was considered to be the MRS loop size, i.e., 150 m and 100m. Nevertheless, like other geophysical methods, ERT has equivalence problems, i.e., non–uniqueness of inversion results. This can be better constrained with more information in the area, e.g., lithology and water content.

Table 7. Detailed information on ERT.

Detailed information		ERT1	ERT2	ERT3	ERT4	ERT5	ERT6	ERT7
Length (m)		890	890	890	890	810	810	810
Position (latitude°) (longitude°)	Start	33.889 102.207	33.929 102.168	33.921 102.145	33.877 102.082	33.864 102.184	33.823 102.227	33.900 101.982
	End	33.881 102.209	33.925 102.160	33.918 102.136	33.881 102.074	33.860 102.191	33.822 102.218	33.903 101.990
Orientation		ES167°	SW242°	SW243°	WN307°	ES130°	SW261°	NE63°

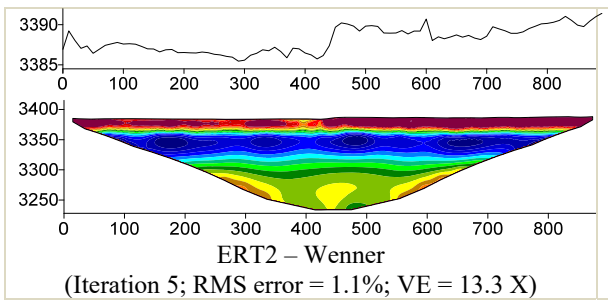

ERT2 – Wenner
(Iteration 5; RMS error = 1.1%; VE = 13.3 X)

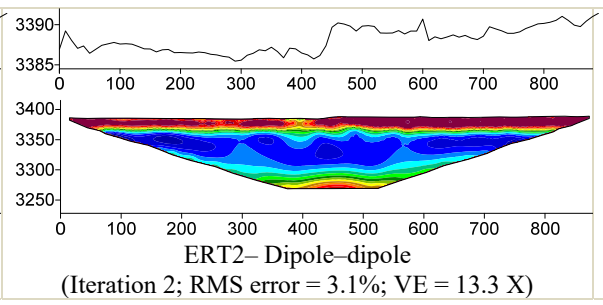

ERT2– Dipole–dipole
(Iteration 2; RMS error = 3.1%; VE = 13.3 X)

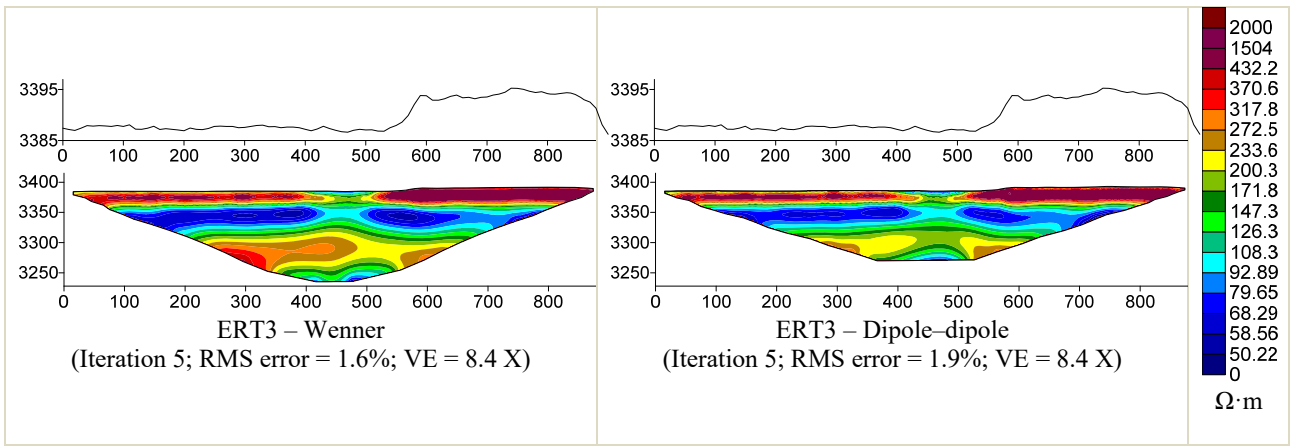

Figure 11. ERT2 and ERT3 measurements and corresponding ground surface elevation and vertical exaggeration (VE).

4.5.3 MRS

Alluvial deposits may be locally highly heterogeneous, but in the study area, they all have high permeability because they are braided river deposits. Besides, in the flat eastern area, there aren't big geographic or geomorphic variations, and the ERT results suggest a roughly regular parallel stratification to surface electrostratigraphy. As such, generally horizontal aquifers are expected in the east, and we didn't use default inversion parameters because they sometimes result in abrupt changes or discontinuities of water content at two near MRS sounding sites. Some excitations were excluded during inversion based on S/N and the mismatch in terms of amplitude, Larmor frequency, and phase. The inversion parameters are listed in Table A5.

The temperature of the water leads to different water densities and viscosities, and influences therefore also hydraulic parameters. In Samovar V6.6, a default temperature of 20 ℃ is used. But in the study area, the average groundwater temperature is 6.2 ℃. Therefore, it is necessary to take the groundwater temperature into account when estimating hydraulic parameters. Thus, based on the eq. 8, a correction factor of 0.69 was used during the inversion process to improve accuracy.

$$K = k\rho g/\eta, \quad (8)$$

Where K is hydraulic conductivity (m/d), k is the permeability of porous media (m^2), ρ is water density (kg/m^3), g is the gravitational acceleration (m/s^2), and η is water viscosity (Pa·s).

MRS3–1 sounding (Fig. 4) was used to calculate the calibration coefficient C_p, because it is the nearest MRS sounding to the borehole ITC_Maqu_1 (shown in Fig. 3a as Core_lithology_analysis) for which pumping test data is available. Using a single point of calibration, the calibration coefficient C_p can be estimated with the uncertainty ≤ 150% (Boucher et al., 2009). The calibrated C_p is 8.78E–09 for T_1 and 8.13E–9 for T_2^*. Fig. 12 shows inversion results of water content and T_1 derived from MRS2–1, MRS3–1, and MRS3–2, and complete results are shown in Fig. A3 in the Appendix. Except for MRS9–2, water mainly concentrates in upper layers, above the 60 meters depth. However, still some of the in-situ water is missing on account of the depth and on account of the current 'window of the technique' sensitive to the larger pore fraction of the in-situ water.

Formatted: Font color: Auto

Formatted: Font color: Auto

Formatted: Font color: Auto

Formatted: Font color: Auto

Deleted: MRS3–1 was used to calculate the calibration coefficient C_p, because it is the nearest MRS sounding to the well (ITC_Maqu_1) for which pumping test data is available.

Detailed results are listed in Table A6 in the Appendix, including T_1, T_2^*, water content, T_1 and T_2^* derived hydraulic conductivities K_{T1}, K_{T2*} and transmissivities T_{T1}, T_{T2*}. In the table, 0.00 and 1000.00 are invalid values for T_2^*. 0.00 and 3000.00 are invalid values for T_1. This un-determination of some parameters may be attributed to the hydrogeological conditions, such as highly heterogeneous lithology and too low signal/noise ratio, and may be eased using Samovar V11.4 which incorporates singular value decomposition. Nevertheless, in highly heterogeneous environments, the un-determination of some parameters may remain with current technology. According to Table A6, except for invalid values, T_1 derived hydraulic conductivity (K_{T1}) ranges from 0.00m/d to 19.64 m/d, T_2^* derived hydraulic conductivity (K_{T2*}) ranges from 0.00 m/d to 210.98 m/d. An order of magnitude difference is observed between the range of K_{T1} and the range of K_{T2*}, which may be due to the big difference between T_1 and T_2^*. Otherwise, more pumping test data are needed to further calibrate C_p. Derived hydraulic conductivity of 0.00 m/d is from the very low water content.

MRS has its own limitations in that the inversion involves equivalence problems, i.e., non–uniqueness of inversion results, and there is a decrease of resolution with depth. In this study, the most serious MRS limitation is that part of the aquifer too deep to be investigated by current MRS instrument implementation. Despite all the mentioned limitations, the MRS did characterize non-invasively the subsurface hydrogeological properties. And there is no ambiguity in terms of quantifying the amount of free water (Lubczynski and Roy, 2003) compared to other hydrogeophysical methods. So information about the amount of free water is the most reliable result we could acquire from MRS. It is expected when more lithology and water content information becomes available, and with the improvement of the MRS inversion technique, the results will become more accurate.

Formatted: Font color: Auto

Formatted: Font color: Auto

Formatted: Font color: Auto

Deleted: for the current technological performance of the MRS technique. Despite limitations observed, MRS does

Deleted: in the area

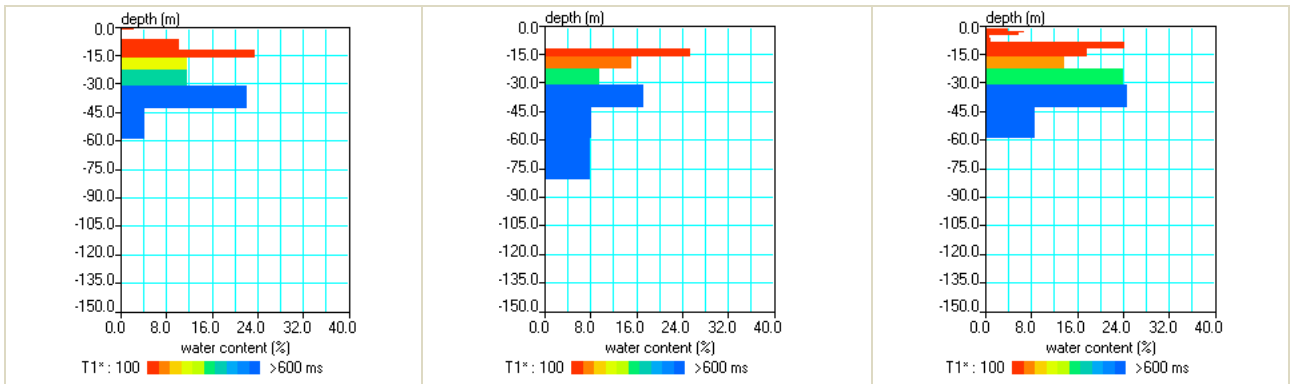

MRS2–1 (S/N = 19.19)	MRS3–1 (S/N = 26.57)	MRS3–2 (S/N = 18.69)

Figure 12. Water content and T_1 derived from MRS2–1, MRS3–1, and MRS3–2.

4.5.4 TEM

Detailed information of ten optimal TEM measurements and inversion parameters are listed in Table 8 and Table A7, respectively. The industrial noise filter was set at 50 Hz, and the amplifier was off. In the study area, using the square loop with a side length of 48 m or 95 m, the maximum time of 1 ms or 4 ms, stack between 5 – 10, and current of 0.8 A or 1.1 A, the TEM method can reach the maximum investigation depth ranging from 150 m to more than 1000 m. For data processing, the invalid data points in field data were first removed, then the field data were smoothed, and the initial model was constructed based on apparent conductance S(h). After that, the process of the inverse problem solution was started. Induced polarization (IP) and superparamagnetic (SPM) effects were not considered in the inversion process. Because of the dead time and the fact that at most sites, a relatively dry layer of sediments exists near the ground surface with a corresponding high resistivity depth interval, the upper 15 m to 30 m of the sounding is lost, although subsequent layered earth modeling attempts filling the gap. The RMS error of the inversion results shown in Fig. 13 is below 2% in the flat area and below 10% in the mountainous area. The results in the mountainous area, i.e., results of TEM6, TEM7, and TEM8, indicate that the resistivity becomes larger in the deep subsurface, and is consistent with our understanding that the bedrock is located at relatively shallow depth from the ground surface. The maximum investigation depth of TEM6 is shallow, only ten time windows were available and resulted in about 150 m investigation depth from the ground surface. This may be due to the local unknown geological condition. In addition to consolidated rock resistivity of the order of 2 kΩ·m to 4 kΩ·m, TEM7 and TEM8 responses may show instances of fracturing, weathering or faulting so that several additional measurements will be needed in the future for confirmation. The rest of the TEM measurements are scattered in the east where it is likely that lake deposits are covered by river deposits on the top. Because the clay silt lithology has a lower resistivity than sand-rich lithology, and Chen et al. (1999) suggested that the ancient lake in Ruoergai Basin was a freshwater or slightly saline lake for most of its life, the decrease of resistivity may indicate the change from river deposits to lake deposits. Table 9 listed the TEM derived depth of river deposits bottom in the east. For TEM0, TEM1, TEM2, TEM3, TEM4, TEM9, the bottom of river deposits are deeper than 100 m, with lake deposits underneath. But for TEM5, the bottom of river deposits is at 50 m deep, followed by 64 m thick lake deposits, with the bedrock down most, and the nearest MRS sounding MRS6-1 indeed shows that there is no free water under 50 m depth.

Table 8. Acquisition parameters of optimal TEM data.

Name	A side length of TEM loop (m)	Latitude (°)	Longitude (°)	Max Time (ms)	Stack	Adjustment of the high voltage protection system (μs)	Current in the transmitting loop (A)
TEM0	48	33.876	102.093	1	6	5	1.1
TEM1	95	33.947	102.135	1	10	7	0.8
TEM2	95	33.865	102.132	4	5	7	0.8
TEM3	95	33.860	102.194	1	10	7	0.8
TEM4	95	33.830	102.225	1	10	7	0.8
TEM5	48	33.790	102.147	1	10	5	1.1
TEM6	95	33.817	102.080	1	5	7	0.8
TEM7	95	33.866	101.983	1	10	7	0.8
TEM8	95	33.884	101.927	1	5	7	0.8
TEM9	95	33.916	102.155	1	10	7	0.8

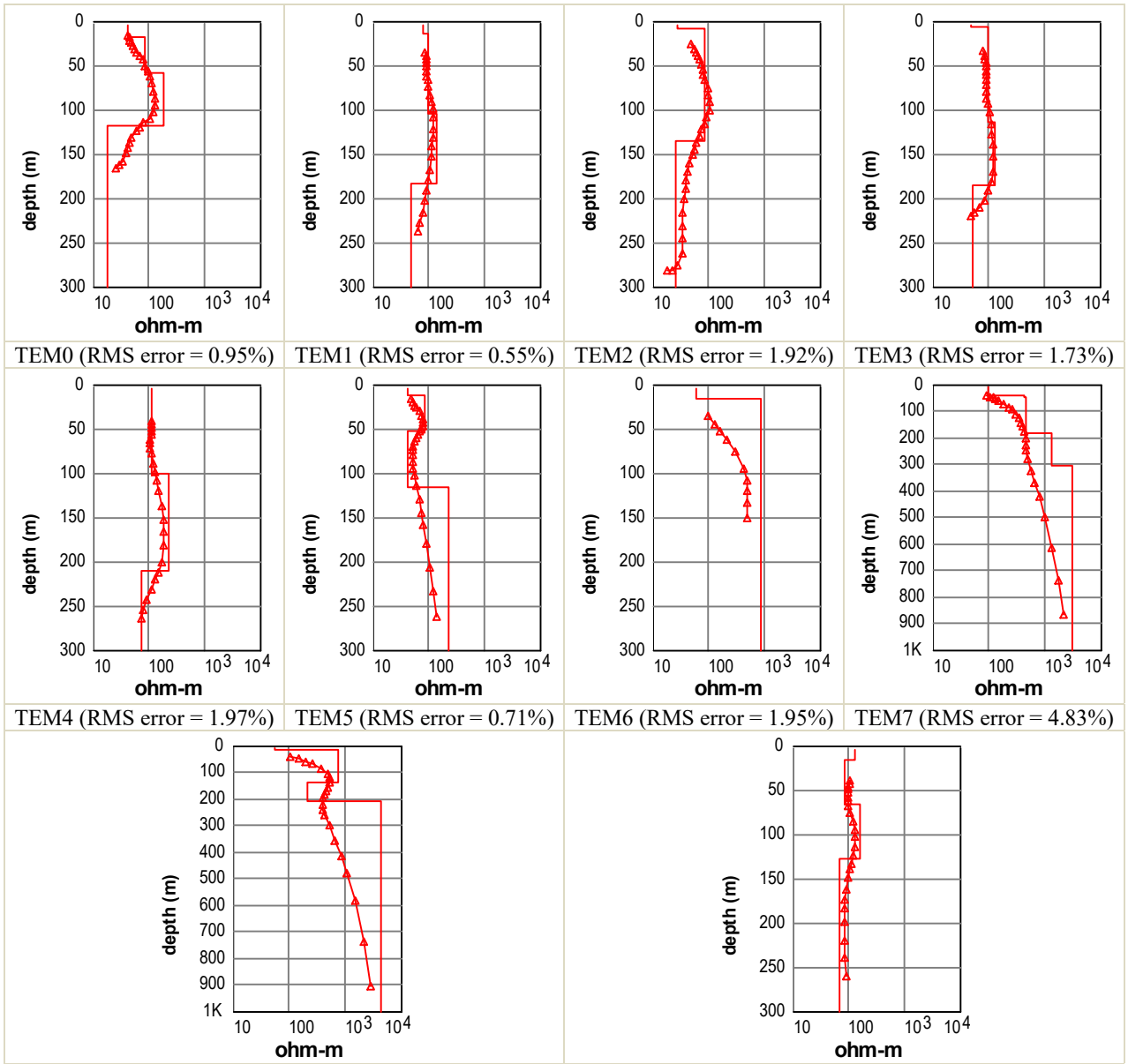

Figure 13. Apparent resistivity and model of TEM.

Table 9. TEM derived depth of river deposits bottom in the east.

Name	Depth of river deposits bottom (m)
TEM0	116
TEM1	181
TEM2	132
TEM3	183
TEM4	208
TEM5	50
TEM9	125

5 Data availability

The raw dataset is archived and freely available in the DANS repository under the link https://doi.org/10.17026/dans-z6t-zpn7 (Li et al., 2020).

6 Conclusion

In this study, we conducted borehole core lithology analysis, altitude survey, soil thickness measurement, hydrogeological survey, and hydrogeophysical survey in the Maqu catchment of the Yellow River source region in the Tibetan Plateau, where little subsurface data are available. Seven DEMs were evaluated using GPS-RTK measured elevation, and ALOS RT1 and ALOS RT2 were proven to have the best overall performance. ALOS RT1 is suggested to be used in future studies because of its slightly better performance and a higher resolution than ALOS RT2. The medium-deep lithology of subsurface down to 32 m below the ground surface, mainly composed of sand, is available only from one borehole ITC_Maqu_1. Soil thicknesses are within 1.2 m in most cases in the west, and the soil thickness decreases as the slope increases based on soil thickness measurements. The hydrogeological survey reveals that groundwater flows from the west to the east, recharging the Yellow River, and the hydraulic conductivity ranges from 0.2 m/d to 12.4 m/d. The hydrogeophysical survey demonstrates the presence of an unconfined aquifer in the east, and water content and hydraulic parameters of that aquifer were estimated at MRS sounding locations. The depth of the Yellow River deposits was derived at TEM sounding positions in the flat eastern area. The raw data set is freely available at https://doi.org/10.17026/dans-z6t-zpn7 (Li et al., 2020). Although water table depths were only measured once or twice, and hydrogeophysical methods, like ERT, TEM, and MRS, have inherent non–uniqueness problems during the inversion process, they all provide valuable information, especially in such data–scarce area as TP. The data in this paper can be used for future set up of a hydrogeological conceptual model and groundwater modeling which will be presented in follow up papers. To our knowledge, this is the first time to conduct such detailed surveys in a TP catchment in order to set up a hydrogeological conceptual and numerical groundwater model. This paper is expected to contribute not only to the hydrogeological conceptual and numerical model of the Maqu catchment at the TP, but also to provide data for hydrogeological and hydrogeophysical communities, and promote interdisciplinary research.

Formatted: Font color: Auto
Formatted: Font color: Auto
Formatted: Font color: Auto
Formatted: Font color: Auto
Deleted: based on
Formatted: Font color: Auto
Formatted: Font color: Auto
Deleted: aquifer
Deleted: The lithology is available in borehole ITC_Maqu_1, and it is mainly composed of sand.
Formatted: Font color: Auto
Formatted: Font color: Auto
Formatted: Font color: Auto
Formatted: Font color: Auto
Formatted: Font color: Auto
Deleted: the
Formatted: Font color: Auto
Formatted: Font color: Auto
Formatted: Font color: Auto
Formatted: Font color: Auto
Deleted: over

Appendix A

Formatted: Font color: Auto

A1 Statistical analysis of seven DEMs in the flat eastern area and the mountainous western area

Table A1. Statistical analysis of seven DEMs in the flat eastern area.

	Min Error * (m)	Max Error (m)	Max Error –Min Error (m)	MAE (Mean Absolute Error) (m)	ME (Mean Error) (m)	Correlation coefficient	RMSE (m)
SRTM	28	44	16	36.916	36.916	0.205	37.148
ASTER V1	–17	41	58	23.539	22.492	0.001	24.902
ASTER V2	–8	52	59	25.455	24.977	0.008	27.626
ASTER V3	4	45	41	28.765	28.765	0.040	30.052
AW3D30	27	43	17	37.522	37.522	0.086	37.788
ALOS RT2	–8	7	15	3.449	1.007	0.234	4.100
ALOS RT1	–8	8	16	3.394	0.947	0.216	4.145

* Error = DEM value – GPS-RTK value

Table A2. Statistical analysis of seven DEMs in the mountainous western area.

	Min Error * (m)	Max Error (m)	Max Error –Min Error (m)	MAE (Mean Absolute Error) (m)	ME (Mean Error) (m)	Correlation coefficient	RMSE (m)
SRTM	22	42	20	31.862	31.862	0.985	32.660
ASTER V1	3	43	39	27.862	27.862	0.956	30.381
ASTER V2	10	55	45	32.631	32.631	0.945	35.828
ASTER V3	13	42	28	29.554	29.554	0.967	31.396
AW3D30	25	44	19	33.016	33.016	0.982	33.807
ALOS RT2	–13	8	21	7.494	–3.753	0.984	8.489
ALOS RT1	–12	7	19	6.968	–3.676	0.985	7.908

* Error = DEM value – GPS-RTK value

A2 Aquifer tests data and derived hydraulic conductivity

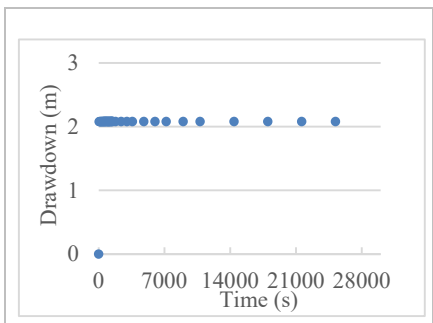

Borehole ITC_Maqu_1: pumping test data; K = 3.6 m/d

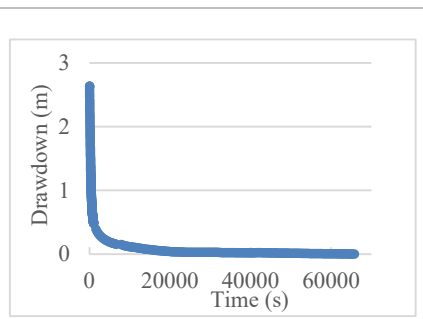

Borehole 6: recovery data; K = 15.6 m/d

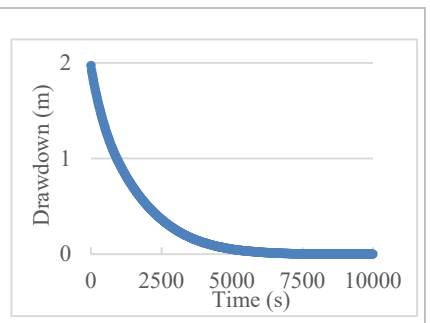

Borehole 23: recovery data; K = 0.1 m/d

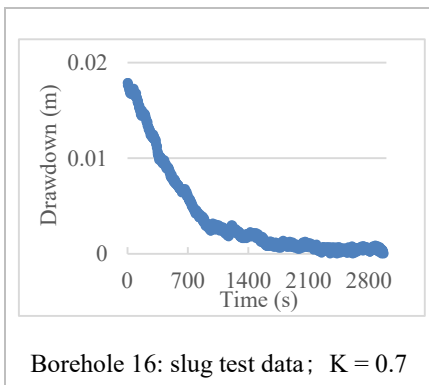

Borehole 16: slug test data; K = 0.7 m/d

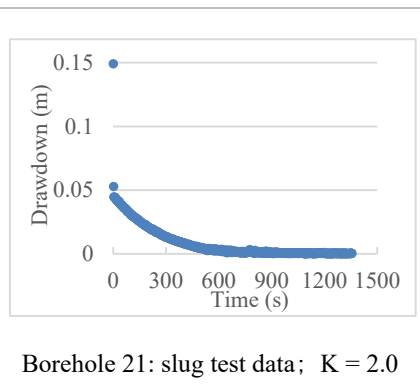

Borehole 21: slug test data; K = 2.0 m/d

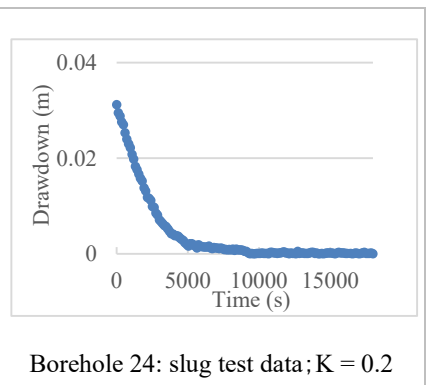

Borehole 24: slug test data; K = 0.2 m/d

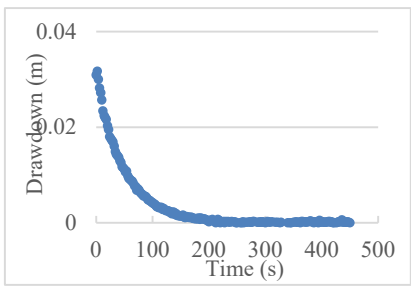

Borehole 26: slug test data; K = 6.2 m/d

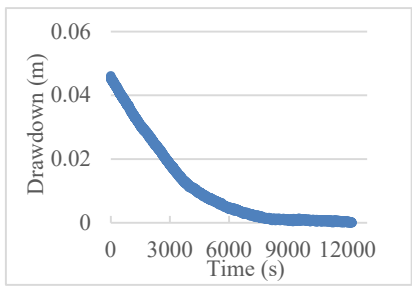

Borehole 27: slug test data; K = 0.2 m/d

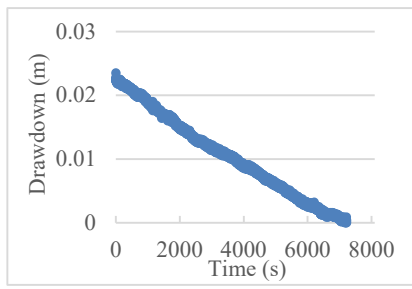

Borehole 32: slug test data; K = 0.2 m/d

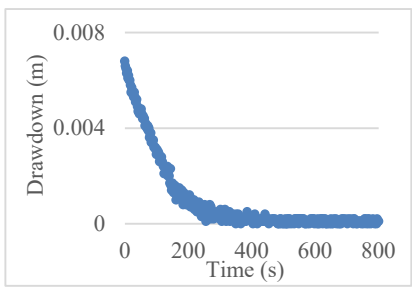

Borehole 33: slug test data; K = 2.6 m/d

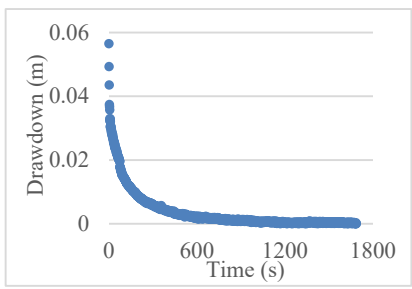

Borehole 34: slug test data; K = 1.4 m/d

Figure A1. Aquifer test data and derived hydraulic conductivity (K).

A3 Inversion parameters for ERT

Table A3. Inversion parameters for ERT.

Parameter	Value
Initial damping factor	0.16
Minimum damping factor	0.015
Convergence limit	5
The minimum change in RMS error	0.4%
Number of iterations	5
Vertical to horizontal flatness filter ratio	1
Number of nodes between adjacent electrodes	2
Increasing of damping factor with depth	1.05
The thickness of the first layer	0.5 m
Factor to increase thickness layer with depth	1.1

A4 Geoelectrical models used for MRS inversion

Table A4. Geoelectrical models used for MRS inversion.

MRS	ERT	Depth (m)		Resistivity from Wenner configuration (ohm–m)
		from	to	
2–1	2	0	20	526
		20	75	86
		75	225	185
3–1, 3–2, 4–1, 4–2	3	0	25	385
		25	70	93
		70	225	213
5–2	4	0	40	90
		40	225	123
1–1, 5–1 8–1, 8–2, 11–1*, 11–2*	5	0	20	290
		20	70	97
		70	225	127
6–1, 7–1, 7–2, 9–1, 9–2	6	0	20	441
		20	60	81
		60	225	193
10–1	7	0	20	99
		20	225	323

* The depth of the third layer is 150m rather than 225m.

A5 ERT measurements and ground surface elevation

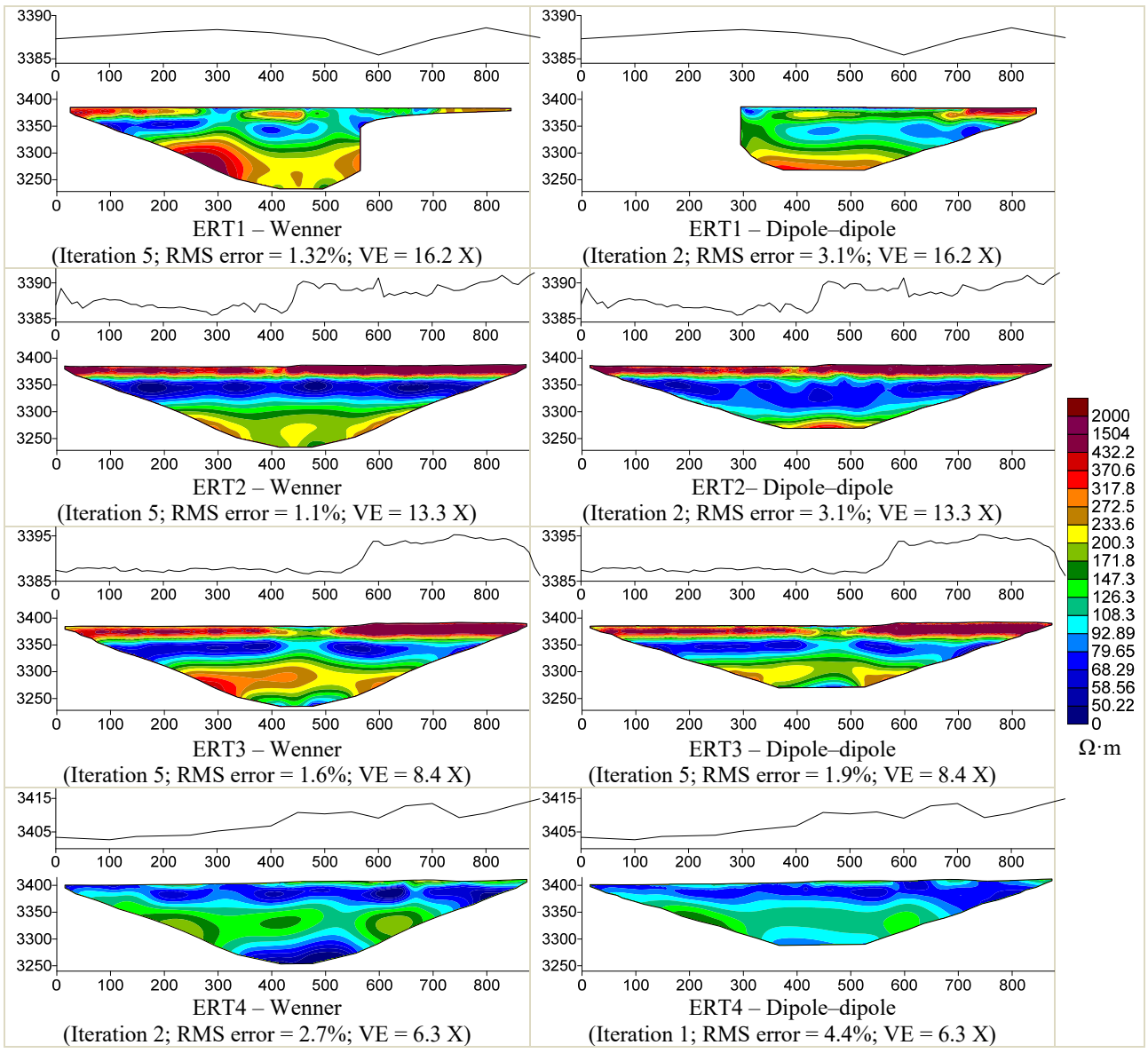

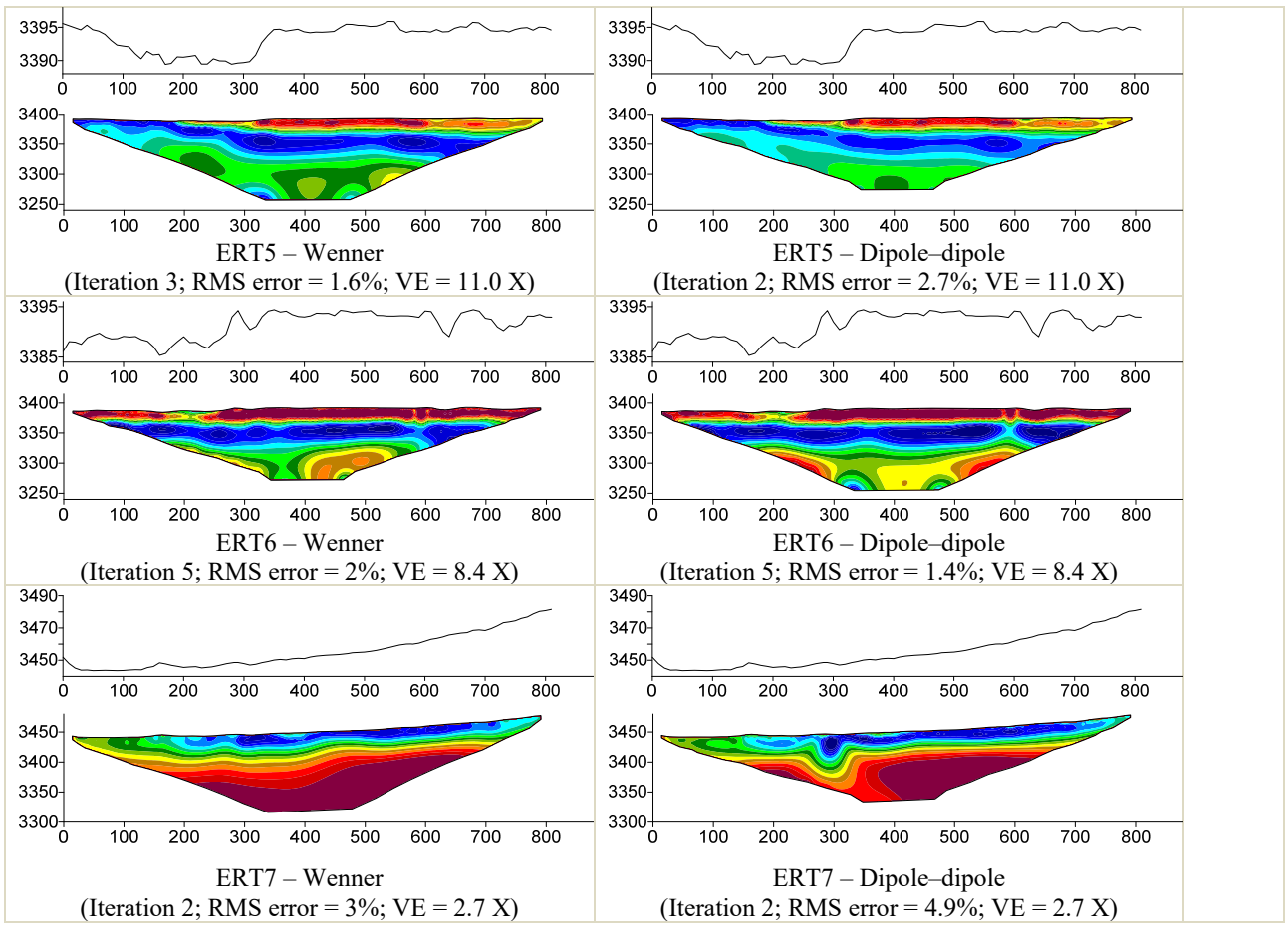

Figure A2. ERT measurements and corresponding ground surface elevation and vertical exaggeration (VE).

A6 Inversion parameters for MRS

Table A5. Inversion parameters for MRS.

MRS	Latitude (°)	Longitude (°)	excluded excitation	Signal processing (200 ms)				Inversion parameters		
				Running aver. filter	Notch filter (50Hz, narrow)	Notch band	Filt. Correction & Centre fixed	Regularization		Model layers
								E, T_2^*	T_1^*	
1–1	33.893	102.205		15				20	1000	16
2–1	33.930	102.171		10				1000	500	15
3–1	33.923	102.149	1	15	√	3.0		500	500	16
3–2	33.922	102.144		15				500	500	16
4–1	33.916	102.135		15	√	3.0		1000	500	16
4–2	33.919	102.124	2	15				1000	500	15

5–1	33.869	102.123		20					500	500	13
5–2	33.875	102.079	1, 16	11					500	500	14
6–1	33.799	102.129	12, 14, 15	15	√	3.0			500	500	16
7–1	33.812	102.197		15					500	500	16
7–2	33.822	102.230		15	√	3.0	√		1000	500	16
8–1	33.863	102.186		15	√	3.0			500	500	15
8–2	33.883	102.209	5, 10	15	√	3.0			1000	500	15
9–1	33.816	102.165		15	√	3.0			1000	500	15
9–2	33.823	102.240	13	15					1000	500	16
10–1	33.901	101.983	16	15	√	3.0	√		500	500	16
11–1	33.875	102.211		15					500	500	16
11–2	33.860	102.164	1	15	√	3.0			1000	500	14

A7 MRS inversion results

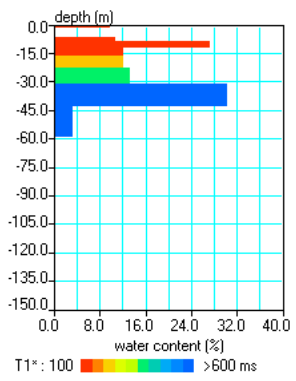

MRS1–1 (S/N = 11.35)

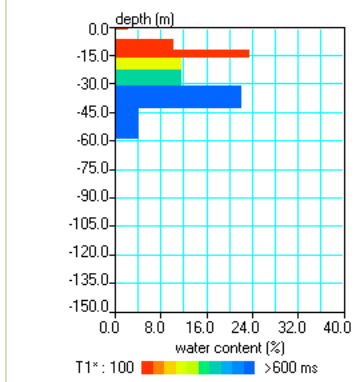

MRS2–1 (S/N = 19.19)

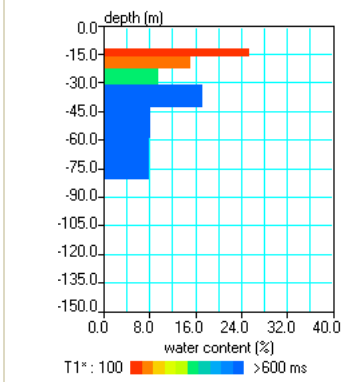

MRS3–1 (S/N = 26.57)

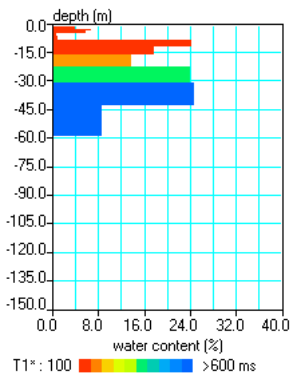

MRS3–2 (S/N = 18.69)

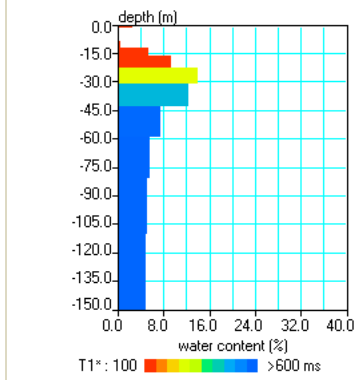

MRS4–1 (S/N = 13.74)

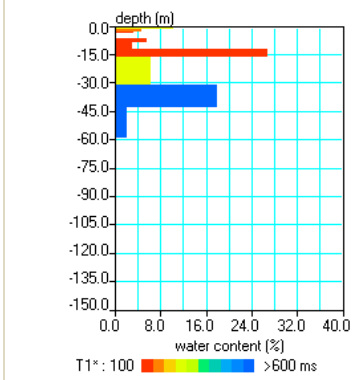

MRS4–2 (S/N = 11.35)

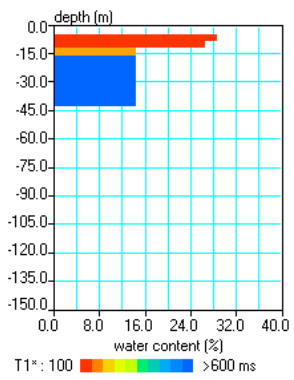

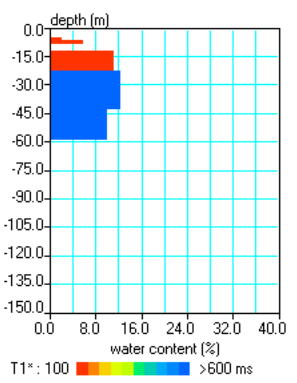

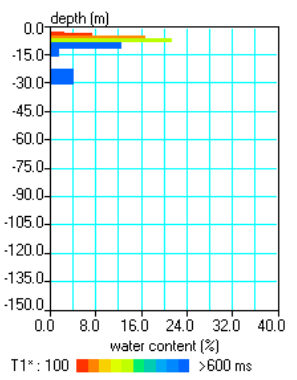

MRS5–1 (S/N = 34.46)

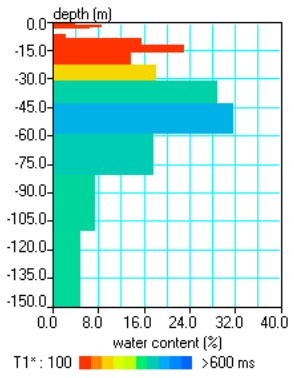

MRS5–2 (S/N = 2.68)

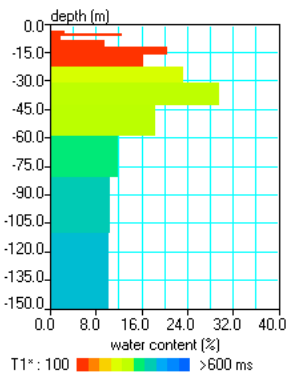

MRS6–1 (S/N = 1.38)

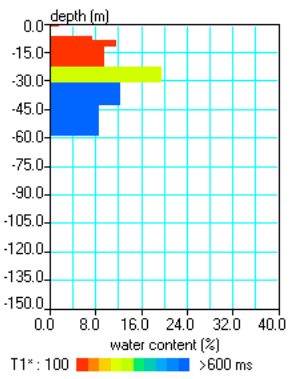

MRS7–1 (S/N = 32.65)

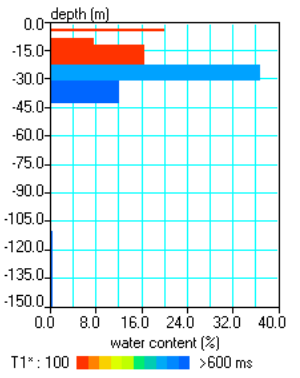

MRS7–2 (S/N = 15.61)

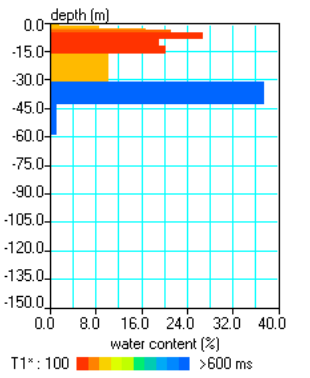

MRS8–1 (S/N = 22.66)

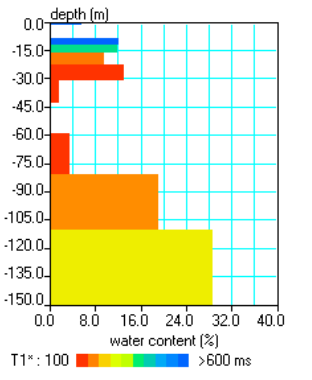

MRS8–2 (S/N = 0.90)

MRS9–1 (S/N = 5.21)

MRS9–2 (S/N = 1.86)

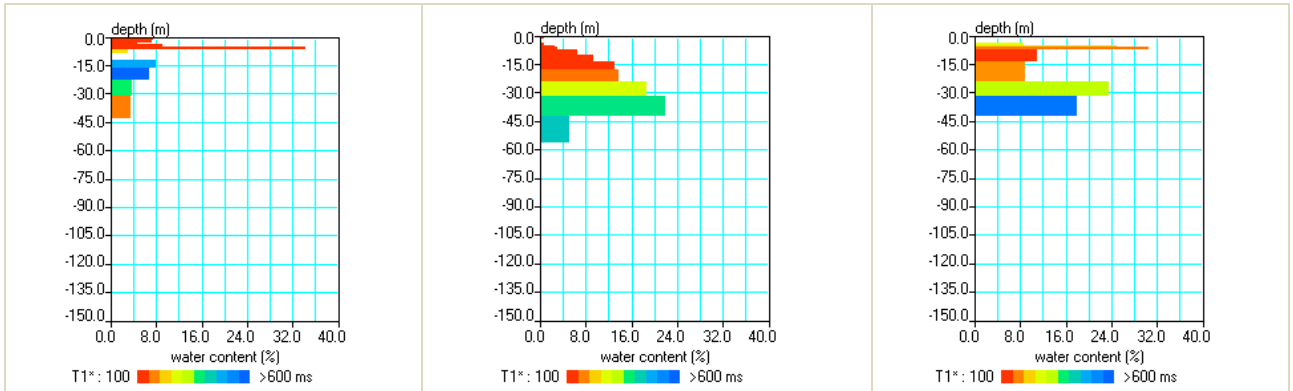

MRS10–1 (S/N = 1.97)	MRS11–1 (S/N = 6.18)	MRS11–2 (S/N = 1.85)

Figure A3. Water content and T1 derived from MRS measurements.

Table A6. MRS inversion results.

MRS	Depth from (m)	Depth to (m)	T_2* (ms)	T_1 (ms)	Water content extrapol (%)	K_{T2*} (m/d)	T_{T2*} (m^2/d)	K_{T1} (m/d)	T_{T1} (m^2/d)
MRS1–1	0.00	1.00	0.00	0.00	0.00	0.00	0.00	0.00	0.00
	1.00	2.00	30.00	50.00	9.84	0.04	0.04	0.13	0.13
	2.00	3.00	0.00	0.00	0.00	0.00	0.00	0.00	0.00
	3.00	4.00	0.00	0.00	0.00	0.00	0.00	0.00	0.00
	4.00	5.00	0.00	0.00	0.00	0.00	0.00	0.00	0.00
	5.00	6.60	0.00	0.00	0.00	0.00	0.00	0.00	0.00
	6.60	9.00	55.20	50.00	10.63	0.16	0.38	0.14	0.34
	9.00	12.30	67.80	50.00	27.25	0.61	2.00	0.36	1.18
	12.30	16.80	45.00	65.50	12.18	0.12	0.54	0.27	1.24
	16.80	23.00	125.10	202.70	12.23	0.93	5.75	2.63	16.28
	23.00	31.50	56.90	372.00	13.38	0.21	1.78	9.69	82.13
	31.50	43.10	60.20	714.90	30.31	0.53	6.17	81.08	940.08
	43.10	58.90	147.80	895.90	3.15	0.33	5.28	13.25	210.28
	58.90	80.70	0.00	0.00	0.00	0.00	0.00	0.00	0.00
	80.70	110.40	0.00	0.00	0.00	0.00	0.00	0.00	0.00
	110.40	150.00	0.00	0.00	0.00	0.00	0.00	0.00	0.00
MRS2–1	0.00	1.00	0.00	0.00	0.00	0.00	0.00	0.00	0.00
	1.00	2.00	30.00	50.00	2.25	0.01	0.01	0.03	0.03
	2.00	3.00	0.00	0.00	0.00	0.00	0.00	0.00	0.00
	3.00	4.00	0.00	0.00	0.00	0.00	0.00	0.00	0.00
	4.00	5.00	0.00	0.00	0.00	0.00	0.00	0.00	0.00
	5.00	6.60	0.00	0.00	0.00	0.00	0.00	0.00	0.00
	6.60	12.30	133.70	50.00	10.15	0.88	5.01	0.13	0.76

	12.30	16.80	46.60	50.00	23.47	0.25	1.11	0.31	1.38
	16.80	23.00	57.00	240.40	11.75	0.18	1.15	3.55	22.03
	23.00	31.50	119.20	417.30	11.70	0.81	6.84	10.66	90.63
	31.50	43.10	47.80	803.80	22.22	0.25	2.85	75.14	871.64
	43.10	58.90	42.10	1274.40	4.14	0.04	0.56	35.22	556.55
	58.90	80.70	0.00	0.00	0.00	0.00	0.00	0.00	0.00
	80.70	110.40	0.00	0.00	0.00	0.00	0.00	0.00	0.00
	110.40	150.00	0.00	0.00	0.00	0.00	0.00	0.00	0.00
MRS3–1	0.00	1.00	1000.00	50.00	3.20	15.52	15.52	0.04	0.04
	1.00	2.00	0.00	0.00	0.00	0.00	0.00	0.00	0.00
	2.00	3.00	0.00	0.00	0.00	0.00	0.00	0.00	0.00
	3.00	4.00	101.20	50.00	0.02	0.00	0.00	0.00	0.00
	4.00	5.00	74.40	50.00	0.03	0.00	0.00	0.00	0.00
	5.00	6.60	30.00	50.00	0.12	0.00	0.00	0.00	0.00
	6.60	9.00	30.00	50.00	0.07	0.00	0.00	0.00	0.00
	9.00	12.30	222.90	50.00	0.00	0.00	0.00	0.00	0.00
	12.30	16.80	65.80	50.00	25.34	0.53	2.39	0.33	1.50
	16.80	23.00	138.10	145.00	15.18	1.40	8.69	1.67	10.34
	23.00	31.50	393.60	376.90	9.49	7.12	60.51	7.05	59.76
	31.50	43.10	119.20	648.60	17.15	1.18	13.69	37.76	437.83
	43.10	58.90	58.10	744.20	8.21	0.13	2.12	23.79	377.49
	58.90	80.70	44.60	782.20	7.98	0.08	1.68	25.54	554.50
	80.70	110.40	0.00	0.00	0.00	0.00	0.00	0.00	0.00
	110.40	150.00	1000.00	50.00	0.00	0.00	0.00	0.00	0.00
MRS3–2	0.00	1.00	0.00	0.00	0.00	0.00	0.00	0.00	0.00
	1.00	2.00	0.00	0.00	0.00	0.00	0.00	0.00	0.00
	2.00	3.00	63.90	50.00	3.99	0.08	0.08	0.05	0.05
	3.00	4.00	56.10	50.00	6.77	0.10	0.10	0.09	0.09
	4.00	5.00	66.10	50.00	5.83	0.12	0.12	0.08	0.08
	5.00	6.60	129.10	50.00	0.74	0.06	0.10	0.01	0.02
	6.60	9.00	663.70	50.00	0.93	1.99	4.78	0.01	0.03
	9.00	12.30	46.00	50.00	24.29	0.25	0.82	0.32	1.05
	12.30	16.80	80.80	50.00	17.68	0.56	2.52	0.23	1.05
	16.80	23.00	167.20	172.50	13.65	1.85	11.46	2.13	13.17
	23.00	31.50	106.50	365.00	24.07	1.32	11.24	16.78	142.22
	31.50	43.10	90.10	742.70	24.70	0.97	11.27	71.31	826.83
	43.10	58.90	94.90	1595.40	8.71	0.38	6.01	116.07	1841.47
	58.90	80.70	30.00	1608.80	0.01	0.00	0.00	0.10	2.11
	80.70	110.40	0.00	0.00	0.00	0.00	0.00	0.00	0.00
	110.40	150.00	0.00	0.00	0.00	0.00	0.00	0.00	0.00

MRS4–1	0.00	1.00	81.10	50.00	3.07	0.10	0.10	0.04	0.04
	1.00	2.00	62.00	50.00	2.66	0.05	0.05	0.03	0.03
	2.00	3.00	0.00	0.00	0.00	0.00	0.00	0.00	0.00
	3.00	4.00	0.00	0.00	0.00	0.00	0.00	0.00	0.00
	4.00	5.00	0.00	0.00	0.00	0.00	0.00	0.00	0.00
	5.00	6.60	0.00	0.00	0.00	0.00	0.00	0.00	0.00
	6.60	9.00	0.00	0.00	0.00	0.00	0.00	0.00	0.00
	9.00	12.30	1000.00	50.00	0.46	2.22	7.34	0.01	0.02
	12.30	16.80	160.70	50.00	5.39	0.67	3.03	0.07	0.32
	16.80	23.00	254.80	50.00	9.27	2.92	18.08	0.12	0.75
	23.00	31.50	208.00	253.90	14.00	2.93	24.93	4.72	40.02
	31.50	43.10	170.80	467.20	12.38	1.75	20.29	14.14	163.90
	43.10	58.90	115.80	594.00	7.50	0.49	7.70	13.85	219.71
	58.90	80.70	75.60	675.70	5.51	0.15	3.33	13.18	286.11
	80.70	110.40	73.60	725.90	5.03	0.13	3.92	13.86	411.77
	110.40	150.00	79.10	747.30	4.88	0.15	5.86	14.28	566.03
MRS4–2	0.00	1.00	757.10	294.20	5.37	14.91	14.91	2.43	2.43
	1.00	2.00	91.10	240.90	10.27	0.41	0.41	3.12	3.12
	2.00	3.00	78.80	149.70	4.57	0.14	0.14	0.54	0.54
	3.00	4.00	289.60	50.00	3.36	1.36	1.36	0.04	0.04
	4.00	5.00	0.00	0.00	0.00	0.00	0.00	0.00	0.00
	5.00	6.60	1000.00	50.00	0.18	0.86	1.38	0.00	0.00
	6.60	9.00	98.90	50.00	5.64	0.27	0.64	0.07	0.18
	9.00	12.30	169.90	50.00	2.99	0.42	1.38	0.04	0.13
	12.30	16.80	36.00	50.00	26.79	0.17	0.76	0.35	1.58
	16.80	31.50	139.10	248.90	6.21	0.58	8.56	2.01	29.61
	31.50	43.10	48.50	1139.20	17.87	0.20	2.36	121.37	1407.91
	43.10	58.90	30.00	1798.40	2.12	0.01	0.15	35.95	568.03
	58.90	80.70	0.00	0.00	0.00	0.00	0.00	0.00	0.00
	80.70	110.40	0.00	0.00	0.00	0.00	0.00	0.00	0.00
	110.40	150.00	0.00	0.00	0.00	0.00	0.00	0.00	0.00
MRS5–1	0.00	1.00	0.00	0.00	0.00	0.00	0.00	0.00	0.00
	1.00	2.00	0.00	0.00	0.00	0.00	0.00	0.00	0.00
	2.00	3.00	0.00	0.00	0.00	0.00	0.00	0.00	0.00
	3.00	4.00	0.00	0.00	0.00	0.00	0.00	0.00	0.00
	4.00	5.00	0.00	0.00	0.00	0.00	0.00	0.00	0.00
	5.00	9.00	168.40	50.00	28.75	3.95	15.80	0.38	1.50
	9.00	12.30	166.00	50.00	26.56	3.55	11.70	0.35	1.15
	12.30	16.80	112.40	179.60	14.43	0.88	3.97	2.43	10.96
	16.80	43.10	129.40	1666.40	14.52	1.18	30.97	210.98	5548.77

	43.10	58.90	0.00	0.00	0.00	0.00	0.00	0.00	0.00
	58.90	80.70	0.00	0.00	0.00	0.00	0.00	0.00	0.00
	80.70	110.40	0.00	0.00	0.00	0.00	0.00	0.00	0.00
	110.40	150.00	0.00	0.00	0.00	0.00	0.00	0.00	0.00
MRS5–2	0.00	1.00	0.00	0.00	0.00	0.00	0.00	0.00	0.00
	1.00	2.00	0.00	0.00	0.00	0.00	0.00	0.00	0.00
	2.00	3.00	0.00	0.00	0.00	0.00	0.00	0.00	0.00
	3.00	4.00	0.00	0.00	0.00	0.00	0.00	0.00	0.00
	4.00	5.00	0.00	0.00	0.00	0.00	0.00	0.00	0.00
	5.00	6.60	30.00	50.00	2.08	0.01	0.01	0.03	0.04
	6.60	9.00	30.00	50.00	5.83	0.03	0.06	0.08	0.18
	9.00	12.30	0.00	0.00	0.00	0.00	0.00	0.00	0.00
	12.30	23.00	198.90	50.00	11.21	2.15	22.99	0.15	1.57
	23.00	43.10	204.40	3000.00	12.31	2.49	50.09	579.99	11657.71
	43.10	58.90	1000.00	885.20	10.05	48.67	768.94	41.19	650.86
	58.90	80.70	0.00	0.00	0.00	0.00	0.00	0.00	0.00
	80.70	110.40	0.00	0.00	0.00	0.00	0.00	0.00	0.00
	110.40	150.00	0.00	0.00	0.00	0.00	0.00	0.00	0.00
MRS6–1	0.00	1.00	0.00	0.00	0.00	0.00	0.00	0.00	0.00
	1.00	2.00	0.00	0.00	0.00	0.00	0.00	0.00	0.00
	2.00	3.00	0.00	0.00	0.00	0.00	0.00	0.00	0.00
	3.00	4.00	1000.00	50.00	2.67	12.91	12.91	0.03	0.03
	4.00	5.00	1000.00	67.70	7.47	36.18	36.18	0.18	0.18
	5.00	6.60	490.70	165.00	16.84	19.64	31.42	2.40	3.75
	6.60	9.00	136.10	334.90	21.46	1.93	4.62	12.59	30.45
	9.00	12.30	30.00	872.30	12.48	0.05	0.18	49.70	164.38
	12.30	16.80	152.00	2859.80	1.68	0.19	0.85	71.88	325.33
	16.80	23.00	0.00	0.00	0.00	0.00	0.00	0.00	0.00
	23.00	31.50	61.20	3000.00	4.28	0.08	0.66	201.54	1707.85
	31.50	43.10	0.00	0.00	0.00	0.00	0.00	0.00	0.00
	43.10	58.90	0.00	0.00	0.00	0.00	0.00	0.00	0.00
	58.90	80.70	0.00	0.00	0.00	0.00	0.00	0.00	0.00
	80.70	110.40	0.00	0.00	0.00	0.00	0.00	0.00	0.00
	110.40	150.00	0.00	0.00	0.00	0.00	0.00	0.00	0.00
MRS7–1	0.00	1.00	0.00	0.00	0.00	0.00	0.00	0.00	0.00
	1.00	2.00	31.30	50.00	3.91	0.02	0.02	0.05	0.05
	2.00	3.00	30.00	50.00	8.56	0.04	0.04	0.11	0.11
	3.00	4.00	42.20	50.00	6.63	0.06	0.06	0.09	0.09
	4.00	5.00	0.00	0.00	0.00	0.00	0.00	0.00	0.00
	5.00	6.60	0.00	0.00	0.00	0.00	0.00	0.00	0.00

	6.60	9.00	1000.00	50.00	2.22	10.75	25.79	0.03	0.07
	9.00	12.30	110.00	50.00	15.57	0.91	3.01	0.20	0.67
	12.30	16.80	51.10	50.00	22.97	0.29	1.31	0.30	1.36
	16.80	23.00	114.00	50.00	13.79	0.87	5.38	0.18	1.12
	23.00	31.50	347.10	215.80	18.17	10.61	90.16	4.43	37.53
	31.50	43.10	177.50	424.70	28.90	4.41	51.17	27.28	316.35
	43.10	58.90	73.40	477.30	31.78	0.83	13.11	37.90	601.29
	58.90	80.70	96.30	434.40	17.70	0.80	17.33	17.48	379.47
	80.70	110.40	583.80	415.50	7.35	12.13	360.34	6.64	197.23
	110.40	150.00	1000.00	412.70	4.80	23.26	920.91	4.28	169.67
MRS7–2	0.00	1.00	0.00	0.00	0.00	0.00	0.00	0.00	0.00
	1.00	2.00	0.00	0.00	0.00	0.00	0.00	0.00	0.00
	2.00	3.00	0.00	0.00	0.00	0.00	0.00	0.00	0.00
	3.00	4.00	0.00	0.00	0.00	0.00	0.00	0.00	0.00
	4.00	5.00	30.00	50.00	2.60	0.01	0.01	0.03	0.03
	5.00	6.60	33.90	50.00	12.48	0.07	0.11	0.16	0.26
	6.60	9.00	70.70	50.00	1.80	0.04	0.10	0.02	0.06
	9.00	12.30	235.30	50.00	9.60	2.57	8.49	0.13	0.42
	12.30	16.80	177.50	50.00	20.48	3.13	14.07	0.27	1.21
	16.80	23.00	95.50	50.00	16.44	0.73	4.50	0.22	1.33
	23.00	31.50	105.80	276.70	23.28	1.26	10.73	9.33	79.06
	31.50	43.10	144.90	326.40	29.58	3.01	34.91	16.49	191.24
	43.10	58.90	158.90	332.60	18.42	2.25	35.60	10.67	169.25
	58.90	80.70	181.90	385.10	11.98	1.92	41.87	9.30	201.85
	80.70	110.40	244.10	435.20	10.57	3.05	90.59	10.47	311.14
	110.40	150.00	372.10	459.20	10.32	6.92	274.04	11.39	451.46
MRS8–1	0.00	1.00	30.00	50.00	7.08	0.03	0.03	0.09	0.09
	1.00	2.00	30.00	50.00	1.57	0.01	0.01	0.02	0.02
	2.00	3.00	0.00	0.00	0.00	0.00	0.00	0.00	0.00
	3.00	4.00	0.00	0.00	0.00	0.00	0.00	0.00	0.00
	4.00	5.00	0.00	0.00	0.00	0.00	0.00	0.00	0.00
	5.00	6.60	0.00	0.00	0.00	0.00	0.00	0.00	0.00
	6.60	9.00	106.20	50.00	7.50	0.41	0.98	0.10	0.24
	9.00	12.30	30.00	50.00	11.66	0.05	0.17	0.15	0.50
	12.30	23.00	141.50	50.00	9.53	0.92	9.90	0.12	1.33
	23.00	31.50	84.90	288.60	19.51	0.68	5.79	8.51	72.31
	31.50	43.10	172.70	683.20	12.46	1.80	20.88	30.44	353.13
	43.10	58.90	45.50	1421.80	8.72	0.09	1.38	92.23	1457.22
	58.90	80.70	0.00	0.00	0.00	0.00	0.00	0.00	0.00
	80.70	110.40	0.00	0.00	0.00	0.00	0.00	0.00	0.00

	110.40	150.00	0.00	0.00	0.00	0.00	0.00	0.00	0.00
MRS8–2	0.00	1.00	0.00	0.00	0.00	0.00	0.00	0.00	0.00
	1.00	2.00	0.00	0.00	0.00	0.00	0.00	0.00	0.00
	2.00	3.00	0.00	0.00	0.00	0.00	0.00	0.00	0.00
	3.00	4.00	0.00	0.00	0.00	0.00	0.00	0.00	0.00
	4.00	5.00	30.00	50.00	20.10	0.09	0.09	0.26	0.26
	5.00	6.60	0.00	0.00	0.00	0.00	0.00	0.00	0.00
	6.60	9.00	0.00	0.00	0.00	0.00	0.00	0.00	0.00
	9.00	12.30	472.90	50.00	7.67	8.31	27.41	0.10	0.33
	12.30	23.00	30.00	50.00	16.64	0.07	0.78	0.22	2.33
	23.00	31.50	61.00	501.30	36.77	0.66	5.63	48.37	411.11
	31.50	43.10	46.00	3000.00	12.13	0.12	1.44	571.34	6627.56
	43.10	58.90	89.50	3000.00	0.12	0.00	0.08	5.82	91.96
	58.90	80.70	0.00	0.00	0.00	0.00	0.00	0.00	0.00
	80.70	110.40	1000.00	3000.00	0.27	1.31	38.82	12.71	377.45
	110.40	150.00	1000.00	3000.00	0.46	2.21	87.61	21.51	851.96
MRS9–1	0.00	1.00	0.00	0.00	0.00	0.00	0.00	0.00	0.00
	1.00	2.00	77.80	200.70	1.55	0.05	0.05	0.33	0.33
	2.00	3.00	100.10	194.30	8.55	0.42	0.42	1.69	1.69
	3.00	4.00	135.40	172.30	16.88	1.50	1.50	2.62	2.62
	4.00	5.00	119.00	136.20	21.18	1.45	1.45	2.06	2.06
	5.00	6.60	108.30	97.80	26.89	1.53	2.44	1.35	2.15
	6.60	9.00	178.40	50.00	26.76	4.13	9.90	0.35	0.84
	9.00	12.30	151.60	50.00	19.09	2.13	7.01	0.25	0.82
	12.30	16.80	54.70	50.00	20.19	0.29	1.32	0.26	1.19
	16.80	31.50	185.30	194.80	10.32	1.72	25.24	2.05	30.15
	31.50	43.10	107.10	839.60	37.63	2.09	24.25	138.81	1610.20
	43.10	58.90	30.00	1165.00	1.21	0.01	0.08	8.58	135.62
	58.90	80.70	0.00	0.00	0.00	0.00	0.00	0.00	0.00
	80.70	110.40	0.00	0.00	0.00	0.00	0.00	0.00	0.00
	110.40	150.00	0.00	0.00	0.00	0.00	0.00	0.00	0.00
MRS9–2	0.00	1.00	57.70	569.30	27.56	0.44	0.44	46.75	46.75
	1.00	2.00	196.70	630.50	5.64	1.06	1.06	11.74	11.74
	2.00	3.00	0.00	0.00	0.00	0.00	0.00	0.00	0.00
	3.00	4.00	0.00	0.00	0.00	0.00	0.00	0.00	0.00
	4.00	5.00	0.00	0.00	0.00	0.00	0.00	0.00	0.00
	5.00	6.60	0.00	0.00	0.00	0.00	0.00	0.00	0.00
	6.60	9.00	0.00	0.00	0.00	0.00	0.00	0.00	0.00
	9.00	12.30	30.00	727.20	12.05	0.05	0.17	33.33	110.25
	12.30	16.80	34.70	400.90	11.97	0.07	0.31	10.07	45.59

	16.80	23.00	45.20	148.00	9.48	0.09	0.58	1.09	6.73
	23.00	31.50	37.40	50.00	13.15	0.09	0.76	0.17	1.46
	31.50	43.10	335.50	50.00	1.71	0.93	10.81	0.02	0.26
	43.10	58.90	0.00	0.00	0.00	0.00	0.00	0.00	0.00
	58.90	80.70	102.60	50.00	3.48	0.18	3.86	0.05	0.99
	80.70	110.40	38.70	163.60	19.05	0.14	4.11	2.67	79.28
	110.40	150.00	33.40	231.40	28.71	0.16	6.14	8.05	319.00
MRS10–1	0.00	1.00	1000.00	50.00	0.86	4.16	4.16	0.01	0.01
	1.00	2.00	1000.00	50.00	7.42	35.95	35.95	0.10	0.10
	2.00	3.00	1000.00	50.00	7.16	34.68	34.68	0.09	0.09
	3.00	4.00	1000.00	50.00	4.78	23.14	23.14	0.06	0.06
	4.00	5.00	64.80	50.00	9.16	0.19	0.19	0.12	0.12
	5.00	6.60	54.30	50.00	34.20	0.49	0.78	0.45	0.70
	6.60	9.00	499.50	225.60	3.07	3.71	8.91	0.82	1.98
	9.00	12.30	0.00	0.00	0.00	0.00	0.00	0.00	0.00
	12.30	16.80	74.20	489.60	7.83	0.21	0.94	9.82	44.44
	16.80	23.00	34.60	681.00	6.68	0.04	0.24	16.21	100.41
	23.00	31.50	371.10	371.60	3.64	2.43	20.62	2.63	22.27
	31.50	43.10	1000.00	152.10	3.42	16.54	191.91	0.41	4.80
	43.10	58.90	0.00	0.00	0.00	0.00	0.00	0.00	0.00
	58.90	80.70	0.00	0.00	0.00	0.00	0.00	0.00	0.00
	80.70	110.40	0.00	0.00	0.00	0.00	0.00	0.00	0.00
	110.40	150.00	0.00	0.00	0.00	0.00	0.00	0.00	0.00
MRS11–1	0.00	1.00	30.00	50.00	0.05	0.00	0.00	0.00	0.00
	1.00	2.00	1000.00	50.00	0.72	3.51	3.51	0.01	0.01
	2.00	3.00	0.00	0.00	0.00	0.00	0.00	0.00	0.00
	3.00	4.00	0.00	0.00	0.00	0.00	0.00	0.00	0.00
	4.00	5.00	30.00	50.00	0.73	0.00	0.00	0.01	0.01
	5.00	6.00	30.00	50.00	2.52	0.01	0.01	0.03	0.03
	6.00	7.50	30.00	50.00	3.14	0.01	0.02	0.04	0.06
	7.50	10.00	30.00	50.00	6.60	0.03	0.07	0.09	0.22
	10.00	13.40	63.50	50.00	9.44	0.18	0.63	0.12	0.42
	13.40	17.90	82.40	50.00	12.96	0.43	1.92	0.17	0.76
	17.90	23.90	82.60	146.00	13.87	0.46	2.75	1.55	9.28
	23.90	31.90	83.60	279.20	18.76	0.64	5.08	7.66	61.25
	31.90	42.50	66.00	393.90	21.99	0.46	4.92	17.85	189.26
	42.50	56.70	50.30	442.70	5.17	0.06	0.90	5.31	75.38
	56.70	75.70	0.00	0.00	0.00	0.00	0.00	0.00	0.00
	75.70	100.00	0.00	0.00	0.00	0.00	0.00	0.00	0.00

MRS11–2	0.00	1.00	0.00	0.00	0.00	0.00	0.00	0.00	0.00
	1.00	2.00	0.00	0.00	0.00	0.00	0.00	0.00	0.00
	2.00	3.00	0.00	0.00	0.00	0.00	0.00	0.00	0.00
	3.00	4.00	0.00	0.00	0.00	0.00	0.00	0.00	0.00
	4.00	5.00	183.90	241.80	8.56	1.40	1.40	2.62	2.62
	5.00	6.00	105.40	214.00	24.84	1.34	1.34	5.95	5.95
	6.00	7.50	107.70	147.50	30.44	1.71	2.57	3.47	5.20
	7.50	13.40	497.60	50.00	11.07	13.28	78.35	0.14	0.85
	13.40	23.90	206.00	166.50	8.81	1.81	19.01	1.28	13.42
	23.90	31.90	149.30	322.90	23.44	2.53	20.25	12.79	102.35
	31.90	42.50	235.70	575.40	17.91	4.82	51.09	31.04	329.00
	42.50	56.70	0.00	0.00	0.00	0.00	0.00	0.00	0.00
	56.70	75.70	0.00	0.00	0.00	0.00	0.00	0.00	0.00
	75.70	100.00	0.00	0.00	0.00	0.00	0.00	0.00	0.00

A8 TEM inversion parameters

Table A7. TEM inversion parameters.

Ignored time windows	Ignored time before (μs)	4
	Ignored time after (μs)	16000
	Use auto protection	yes
Adjust cut off ramp	Use cut–off ramp	yes
Regularizing algorithm	Low	
Variation's limits	Resistivity (ohm–m)	0.1–4000
	Thickness (m)	0.25–1000
Smooth field data	Styles	Limited
	Tension	Middle
Transformation resolution	Middle	

Author contributions. ML, ZS, YZ, MWL, JR, LY, HQ, ZL, JC, LH, HZ, TV, JMS, HJHF contributed to the design of this research. ML, JR, LY, HQ, ZL, JC, KH, QZ, PX, FL, KL, YL carried out the fieldwork. All co-authors revised the manuscript and contributed to the writing.

Competing interests. All authors declare that there are no conflicts of interests.

Acknowledgments. We acknowledge the financial support from the National Natural Science Foundation of China (grant no. 41971033), the ESA MOST Dragon IV Program (Monitoring and Modelling Climate Change in Water, Energy and Carbon Cycles in the Pan-Third Pole Environment), the Second Tibetan Plateau Scientific Expedition and Research (STEP) program (grant no. 2019QZKK0103), and Fundamental Research Funds for the Central Universities (300102298307, 300102299305).

Formatted: Font color: Auto

Formatted: Font color: Auto

We thank Prof. Mark van der Meijde from the University of Twente, the staff of Maqu Water Authority, and Director Yang of Hequ stud farm for their great supports for fieldwork.

Deleted: We acknowledge the financial support from Fundamental Research Funds for the Central Universities (300102298307, 300102299305). We thank Chang'an University, ITC, the University of Twente, and Prof. Mark van der Meijde from the University of Twente for their supports, as well as the local government in Maqu for their assistance during fieldwork. This work was also supported in part by the ESA MOST Dragon IV Program (Monitoring and Modelling Climate Change in Water, Energy and Carbon Cycles in the Pan-Third Pole Environment).

Formatted: Font color: Auto

References

Agarwal, R. G.: A new method to account for producing time effects when drawdown type curves are used to analyze pressure buildup and other test data, SPE Paper 9289 presented at the 55th SPE Annual Technical Conference and Exhibition, Dallas, Texas, 1980.

Bernard, J.: Instruments and field work to measure a magnetic resonance sounding, Boletin Geologico y Minero, 118, 459-472, 2007.

Boucher, M., Favreau, G., Vouillamoz, J.-M., Nazoumou, Y., and Legchenko, A.: Estimating specific yield and transmissivity with magnetic resonance sounding in an unconfined sandstone aquifer (Niger), Hydrogeol. J., 17, 1805,doi:10.1007/s10040-009-0447-x, 2009.

Boulton, N. S.: Analysis of data from non-equilibrium pumping tests allowing for delayed yield from storage, Proc. Inst. Civil Eng., 26, 469-482,doi:10.1680/iicep.1963.10409, 1963.

Bouwer, H. and Rice, R.: A slug test for determining hydraulic conductivity of unconfined aquifers with completely or partially penetrating wells, Water Resour. Res., 12, 423-428,doi:10.1029/WR012i003p00423, 1976.

Braun, M. and Yaramanci, U.: Inversion of resistivity in magnetic resonance sounding, J. Appl. Geophys., 66, 151-164,doi:10.1016/j.jappgeo.2007.12.004, 2008.

Chambers, J., Wilkinson, P., Uhlemann, S., Sorensen, J., Roberts, C., Newell, A., Ward, W., Binley, A., Williams, P., and Gooddy, D.: Derivation of lowland riparian wetland deposit architecture using geophysical image analysis and interface detection, Water Resour. Res., 50, 5886-5905,doi:10.1002/2014WR015643, 2014.

Chang, D. Z.: Preliminary analysis and research on the Yellow River water resources in Maqu wetland, Gansu Water Conservancy and Hydropower Technology, 45, 8-10, 2009.

Chen, F., Bloemendal, J., Zhang, P., and Liu, G.: An 800 ky proxy record of climate from lake sediments of the Zoige Basin, eastern Tibetan Plateau, Palaeogeogr. Palaeoclimatol. Palaeoecol., 151, 307-320,doi:10.1016/S0031-0182(99)00032-2, 1999.

Chirindja, F. J., Dahlin, T., Perttu, N., Steinbruch, F., and Owen, R.: Combined electrical resistivity tomography and magnetic resonance sounding investigation of the surface-water/groundwater interaction in the Urema Graben, Mozambique, Hydrogeol. J., 24, 1583-1592,doi:10.1007/s10040-016-1422-y, 2016.

Dente, L., Vekerdy, Z., Wen, J., and Su, Z.: Maqu network for validation of satellite-derived soil moisture products, Int. J. Appl. Earth Obs. Geoinf., 17, 55-65,doi:10.1016/j.jag.2011.11.004, 2012.

Descloitres, M., Ruiz, L., Sekhar, M., Legchenko, A., Braun, J. J., Mohan Kumar, M., and Subramanian, S.: Characterization of seasonal local recharge using electrical resistivity tomography and magnetic resonance sounding, Hydrol. Process., 22, 384-394,doi:10.1002/hyp.6608, 2008.

Descloitres, M., Séguis, L., Wubda, M., and Legchenko, A.: Discrimination of rocks with different hydrodynamic properties using MRS, EM and resistivity methods, Near Surface 2007-13th EAGE European Meeting of Environmental and Engineering Geophysics, 2007.

Di Napoli, R., Aiuppa, A., Sulli, A., Caliro, S., Chiodini, G., Acocella, V., Ciraolo, G., Di Vito, M., Interbartolo, F., and Nasello, C.: Hydrothermal fluid venting in the offshore sector of Campi Flegrei caldera: A geochemical, geophysical, and volcanological study, Geochem., Geophys., Geosyst., 17, 4153-4178,doi:10.1002/2016GC006494, 2016.

Fikos, I., Vargemezis, G., Zlotnicki, J., Puertollano, J., Alanis, P., Pigtain, R., Villacorte, E., Malipot, G., and Sasai, Y.: Electrical resistivity tomography study of Taal volcano hydrothermal system, Philippines, Bull. Volcanol., 74, 1821-1831,doi:10.1007/s00445-012-0638-5, 2012.

Fujita, K., Suzuki, R., Nuimura, T., and Sakai, A.: Performance of ASTER and SRTM DEMs, and their potential for assessing glacial lakes in the Lunana region, Bhutan Himalaya, J. Glaciol., 54, 220-228,doi:10.3189/002214308784886162, 2008.

Gao, S., Jin, H., Bense, V. F., Wang, X., and Chai, X.: Application of electrical resistivity tomography for delineating permafrost hydrogeology in the headwater area of Yellow River on Qinghai-Tibet Plateau, SW China, Hydrogeol. J., 27, 1725-1737,doi:10.1007/s10040-019-01942-z, 2019.

Gonçalves, R. M. D.: Hydrochemical water prediction (water quality) with transient electromagnetic soundings (TEM), 2012. Citeseer, 2012.

Graham, D. N. and Butts, M. B.: Flexible, integrated watershed modelling with MIKE SHE. In: Watershed models, 2005.

Grohmann, C. H.: Evaluation of TanDEM-X DEMs on selected Brazilian sites: Comparison with SRTM, ASTER GDEM and ALOS AW3D30, Remote Sens. Environ., 212, 121-133, 2018.

Haile, K. H.: Estimation of terrestrial water storage in the upper reach of Yellow River, University of Twente Faculty of Geo-Information and Earth Observation (ITC), 2011.

Healy, R. W., Winter, T. C., LaBaugh, J. W., and Franke, O. L.: Water budgets: foundations for effective water-resources and environmental management, US Geological Survey Reston, Virginia, 2007.

Hebeler, F. and Purves, R. S.: The influence of elevation uncertainty on derivation of topographic indices, Geomorphology, 111, 4-16, 2009.

Herckenrath, D., Auken, E., Christiansen, L., Behroozmand, A. A., and Bauer-Gottwein, P.: Coupled hydrogeophysical inversion using time-lapse magnetic resonance sounding and time-lapse gravity data for hydraulic aquifer testing: Will it work in practice?, Water Resour. Res., 48,doi:10.1029/2011WR010411, 2012.

Huang, X., Deng, J., Wang, W., Feng, Q., and Liang, T.: Impact of climate and elevation on snow cover using integrated remote sensing snow products in Tibetan Plateau, Remote Sens. Environ., 190, 274-288,doi:10.1016/j.rse.2016.12.028, 2017.

Immerzeel, W. W., Droogers, P., De Jong, S., and Bierkens, M.: Large-scale monitoring of snow cover and runoff simulation in Himalayan river basins using remote sensing, Remote Sens. Environ., 113, 40-49,doi:10.1016/j.rse.2008.08.010, 2009.

Immerzeel, W. W., Van Beek, L. P., and Bierkens, M. F.: Climate change will affect the Asian water towers, Scieas., 328, 1382-1385,doi:10.1126/science.1183188, 2010.

Jiang, F., Dong, L., and Dai, Q.: Electrical resistivity imaging inversion: An ISFLA trained kernel principal component wavelet neural network approach, Neural Networks, 104, 114-123,doi:10.1016/j.neunet.2018.04.012, 2018.

Jiao, J. J., Zhang, X., Liu, Y., and Kuang, X.: Increased water storage in the Qaidam Basin, the North Tibet Plateau from GRACE gravity data, PloS one, 10, e0141442,doi:10.1371/journal.pone.0141442, 2015.

Kang, S., Xu, Y., You, Q., Flügel, W.-A., Pepin, N., and Yao, T.: Review of climate and cryospheric change in the Tibetan Plateau, Environ. Res. Lett., 5, 015101,doi:10.1088/1748-9326/5/1/015101, 2010.

Kenyon, W., Howard, J., Sezginer, A., Straley, C., Matteson, A., Horkowitz, K., and Ehrlich, R.: Pore-size distribution and NMR in microporous cherty sandstones, SPWLA 30th Annual Logging Symposium, 1989.

Kuang, X. and Jiao, J. J.: Review on climate change on the Tibetan Plateau during the last half century, J. Geophys. Res.: Atmos., 121, 3979-4007,doi:10.1002/2015JD024728, 2016.

Lachassagne, P., Baltassat, J.-M., Legchenko, A., and de Gramont, H. M.: The links between MRS parameters and the hydrogeological parameters, Near Surf. Geophys., 3, 259-265,doi:10.3997/1873-0604.2005021, 2005.

Legchenko, A., Baltassat, J.-M., Beauce, A., and Bernard, J.: Nuclear magnetic resonance as a geophysical tool for hydrogeologists, J. Appl. Geophys., 50, 21-46,doi:10.1016/S0926-9851(02)00128-3, 2002.

Legchenko, A., Baltassat, J. M., Bobachev, A., Martin, C., Robain, H., and Vouillamoz, J. M.: Magnetic resonance sounding applied to aquifer characterization, Groundwater, 42, 363-373,doi:10.1111/j.1745-6584.2004.tb02684.x, 2004.

Legchenko, A., Miège, C., Koenig, L. S., Forster, R. R., Miller, O., Solomon, D., Schmerr, N., Montgomery, L., Ligtenberg, S., and Brucker, L.: Estimating water volume stored in the south-eastern Greenland firn aquifer using magnetic-resonance soundings, J. Appl. Geophys., 150, 11-20,doi:10.1016/j.jappgeo.2018.01.005, 2018.

Legchenko, A. V. and Shushakov, O. A.: Inversion of surface NMR data, Geophysics, 63, 75-84,doi:10.1190/1.1444329, 1998.

Li, M., Zeng, Y., Maciek W., L., Su, Z., and Qian, H.: 2018-2019 dataset in Maqu, the Tibetan Plateau., doi:10.17026/dans-z6t-zpn7, 2020.

Loke, M. H.: Electrical imaging surveys for environmental and engineering studies. User's Manual for Res2dinv, 1999. 1999.

Lubczynski, M. and Roy, J.: Hydrogeological interpretation and potential of the new magnetic resonance sounding (MRS) method, J. Hydrol., 283, 19-40,doi:10.1016/S0022-1694(03)00170-7, 2003.

Lubczynski, M. and Roy, J.: Magnetic resonance sounding: New method for ground water assessment, Groundwater, 42, 291-309,doi:10.1111/j.1745-6584.2004.tb02675.x, 2004.

Lubczynski, M. and Roy, J.: Use of MRS for hydrogeological system parameterization and modeling, Boletin Geologico y Minero, 118, 509-530, 2007.

McClymont, A. F., Roy, J. W., Hayashi, M., Bentley, L. R., Maurer, H., and Langston, G.: Investigating groundwater flow paths within proglacial moraine using multiple geophysical methods, J. Hydrol., 399, 57-69,doi:10.1016/j.jhydrol.2010.12.036, 2011.

McCormack, T., O'Connell, Y., Daly, E., Gill, L., Henry, T., and Perriquet, M.: Characterisation of karst hydrogeology in Western Ireland using geophysical and hydraulic modelling techniques, J. Hydrol.: Reg. Stud., 10, 1-17,doi:10.1016/j.ejrh.2016.12.083, 2017.

Nabighian, M. N. and Macnae, J. C.: Time domain electromagnetic prospecting methods, Electromagnetic methods in applied geophysics, 2, 427-509, 1991.

Nan, X., Li, A., Bian, J., and Zhang, Z.: Comparison of the accuracy between SRTM and ASTER GDEM over typical mountain area: A case study in the Eastern Qinghai-Tibetan Plateau, J. Geo-Inf. Sci, 17, 91-98,doi:10.3724/SP.J.1047.2015.00091, 2015.

Nielsen, M. R., Hagensen, T. F., Chalikakis, K., and Legchenko, A.: Comparison of transmissivities from MRS and pumping tests in Denmark, Near Surf. Geophys., 9, 211-223,doi:10.3997/1873-0604.2010071, 2011.

Niu, F., Yin, G., Luo, J., Lin, Z., and Liu, M.: Permafrost distribution along the Qinghai-Tibet Engineering Corridor, China using high-resolution statistical mapping and modeling integrated with remote sensing and GIS, Remote Sens., 10, 215,doi:10.3390/rs10020215, 2018.

Peel, M. C., Finlayson, B. L., and McMahon, T. A.: Updated world map of the Köppen-Geiger climate classification, Hydrol. Earth Syst. Sci., 11, 1633–1644,doi:10.5194/hess-11-1633-2007, 2007.

Pérez-Bielsa, C., Lambán, L. J., Plata, J. L., Rubio, F. M., and Soto, R.: Characterization of a karstic aquifer using magnetic resonance sounding and electrical resistivity tomography: a case-study of Estaña Lakes (northern Spain), Hydrogeol. J., 20, 1045-1059,doi:10.1007/s10040-012-0839-1, 2012.

Plata, J. and Rubio, F.: Basic theory of the magnetic resonance sounding method, Boletin Geologico y minero, 118, 441-458, 2007.

Plata, J. L. and Rubio, F. M.: The use of MRS in the determination of hydraulic transmissivity: The case of alluvial aquifers, J. Appl. Geophys., 66, 128-139,doi:10.1016/j.jappgeo.2008.04.001, 2008.

Qu, B., Zhang, Y., Kang, S., and Sillanpaa, M.: Water quality in the Tibetan Plateau: Major ions and trace elements in rivers of the "Water Tower of Asia", Sci. Total Environ., 649, 571-581,doi:10.1016/j.scitotenv.2018.08.316, 2019.

Roy, J., Rouleau, A., Chouteau, M., and Bureau, M.: Widespread occurrence of aquifers currently undetectable with the MRS technique in the Grenville geological province, Canada, J. Appl. Geophys., 66, 82-93,doi:10.1016/j.jappgeo.2008.04.006, 2008.

Schoorl, J., Claessens, L., Lopez Ulloa, M., De Koning, G., and Veldkamp, A.: Geomorphological analysis and scenario modelling in the Noboa–Pajan area, Manabi province, Ecuador, Zeitschrift Fur Geomorfologie, 145, 105-118, 2006.

Schoorl, J., Veldkamp, A., and Bouma, J.: Modeling water and soil redistribution in a dynamic landscape context, Soil Sci. Soc. Am. J., 66, 1610-1619, 2002.

Seevers, D.: A nuclear magnetic method for determining the permeability of sandstones, SPWLA 7th Annual Logging Symposium, Tulsa, Oklahoma, 1966.

Shangguan, W., Hengl, T., de Jesus, J. M., Yuan, H., and Dai, Y.: Mapping the global depth to bedrock for land surface modeling, J. Adv. Model Earth Sy., 9, 65-88,doi:10.1002/2016MS000686, 2017.

Steelman, C., Kennedy, C., and Parker, B.: Geophysical conceptualization of a fractured sedimentary bedrock riverbed using ground-penetrating radar and induced electrical conductivity, J. Hydrol., 521, 433-446,doi:10.1016/j.jhydrol.2014.12.001, 2015.

Su, Z., De Rosnay, P., Wen, J., Wang, L., and Zeng, Y.: Evaluation of ECMWF's soil moisture analyses using observations on the Tibetan Plateau, J. Geophys. Res.: Atmos., 118, 5304-5318,doi:10.1002/jgrd.50468, 2013.

Su, Z., Wen, J., Dente, L., Velde, R., Wang, L., Ma, Y., Yang, K., and Hu, Z.: The Tibetan Plateau observatory of plateau scale soil moisture and soil temperature (Tibet-Obs) for quantifying uncertainties in coarse resolution satellite and model products, Hydrol. Earth Syst. Sci., 15, 2303-2316,doi:10.5194/hess-15-2303-2011, 2011.

Vouillamoz, J.-M., Chatenoux, B., Mathieu, F., Baltassat, J.-M., and Legchenko, A.: Efficiency of joint use of MRS and VES to characterize coastal aquifer in Myanmar, J. Appl. Geophys., 61, 142-154,doi:10.1016/j.jappgeo.2006.06.003, 2007.

Vouillamoz, J.-M., Descloitres, M., Bernard, J., Fourcassier, P., and Romagny, L.: Application of integrated magnetic resonance sounding and resistivity methods for borehole implementation. A case study in Cambodia, J. Appl. Geophys., 50, 67-81,doi:10.1016/S0926-9851(02)00130-1, 2002.

Vouillamoz, J.-M., Favreau, G., Massuel, S., Boucher, M., Nazoumou, Y., and Legchenko, A.: Contribution of magnetic resonance sounding to aquifer characterization and recharge estimate in semiarid Niger, J. Appl. Geophys., 64, 99-108, 2008.

Vouillamoz, J.-M., Lawson, F., Yalo, N., and Descloitres, M.: The use of magnetic resonance sounding for quantifying specific yield and transmissivity in hard rock aquifers: The example of Benin, J. Appl. Geophys., 107, 16-24, 2014.

Vouillamoz, J.-M., Sokheng, S., Bruyere, O., Caron, D., and Arnout, L.: Towards a better estimate of storage properties of aquifer with magnetic resonance sounding, J. Hydrol., 458, 51-58,doi:10.1016/j.jhydrol.2012.06.044, 2012.

Vouillamoz, J., Legchenko, A., Albouy, Y., Bakalowicz, M., Baltassat, J., and Al-Fares, W.: Localization of saturated karst aquifer with magnetic resonance sounding and resistivity imagery, Groundwater, 41, 578-586,doi:10.1111/j.1745-6584.2003.tb02396.x, 2003.

Wang, Q., Jin, H., Zhang, T., Cao, B., Peng, X., Wang, K., Xiao, X., Guo, H., Mu, C., and Li, L.: Hydro-thermal processes and thermal offsets of peat soils in the active layer in an alpine permafrost region, NE Qinghai-Tibet plateau, Glob. Planet. Change, 156, 1-12,doi:10.1016/j.gloplacha.2017.07.011, 2017.

Wang, W.: Strategy of ecological protection for water source supply areas of the Yellow River in southern Gansu Province, Yangtze River, 39, 25-27, 2008.

Wang, Y., Wang, S., Xue, B., Ji, L., Wu, J., Xia, W., Pan, H., Zhang, P., and Chen, F.: Sedimentological evidence of the piracy of fossil Zoige Lake by the Yellow River, Chinese Sci. Bull., 40, 1539-1544,doi:CNKI: SUN: JXTW.0.1995-18-008, 1995.

Wei, Y. and Fang, Y.: Spatio-temporal characteristics of global warming in the Tibetan Plateau during the last 50 years based on a generalised temperature zone-elevation model, PloS one, 8,doi:10.1371/journal.pone.0060044, 2013.

Xiang, L., Wang, H., Steffen, H., Wu, P., Jia, L., Jiang, L., and Shen, Q.: Groundwater storage changes in the Tibetan Plateau and adjacent areas revealed from GRACE satellite gravity data, Earth Planet. Sci. Lett., 449, 228-239,doi:10.1016/j.epsl.2016.06.002, 2016.

Xu, Y., Ramanathan, V., and Washington, W.: Observed high-altitude warming and snow cover retreat over Tibet and the Himalayas enhanced by black carbon aerosols, Atmos. Chem. Phys., 16, 1303-1315,doi:10.5194/acp-16-1303-2016, 2016.

Xue, B., Wang, S., Xia, W., Wu, J., Wang, Y., Qian, J., Hu, S., Wu, Y., and Zhang, P.: The uplifting and environmental change of Qinghai-Xizang (Tibetan) Plateau in the past 0.9 Ma inferred from core RM of Zoige Basin, Sci. China Ser. D, 41, 165-170,doi:10.1007/BF02932436, 1998.

Yan, F., Shangguan, W., Zhang, J., and Hu, B.: Depth-to-bedrock map of China at a spatial resolution of 100 meters, Sci. Data, 7, 1-13,doi:10.1038/s41597-019-0345-6, 2020.

Yang, K.: Observed Regional Climate Change in Tibet over the Last Decades. In: Oxford Research Encyclopedia of Climate Science, 2017.

Yao, T., Qin, D., Shen, Y., Zhao, L., Wang, N., and Lu, A.: Cryospheric changes and their impacts on regional water cycle and ecological conditions in the Qinghai-Tibetan Plateau, Chin. J. Nat., 35, 179-186,doi:10.3969/j.issn.0253-9608.2013.03.004, 2013.

Yao, T., Xue, Y., Chen, D., Chen, F., Thompson, L., Cui, P., Koike, T., Lau, W. K.-M., Lettenmaier, D., and Mosbrugger, V.: Recent Third Pole's rapid warming accompanies cryospheric melt and water cycle intensification and interactions between monsoon and environment: Multidisciplinary approach with observations, modeling, and analysis, B. Am. Meteorol. Soc., 100, 423-444,doi:10.1175/BAMS-D-17-0057.1, 2019.

Ye, Q., Bolch, T., Naruse, R., Wang, Y., Zong, J., Wang, Z., Zhao, R., Yang, D., and Kang, S.: Glacier mass changes in Rongbuk catchment on Mt. Qomolangma from 1974 to 2006 based on topographic maps and ALOS PRISM data, J. Hydrol., 530, 273-280, 2015.

Ye, Q., Shi, J., Cheng, X., Li, X., and Hochschild, V.: Application of ALOS Data in Studying Alpine Glaciers in the Mt. Himalayas on the Tibetan Plateau, 1349-113X, 2011.

You, Y., Yu, Q., Pan, X., Wang, X., and Guo, L.: Application of electrical resistivity tomography in investigating depth of permafrost base and permafrost structure in Tibetan Plateau, Cold Reg. Sci. Technol., 87, 19-26,doi:10.1016/j.coldregions.2012.11.004, 2013.

Zeng, Y., Su, Z., Van der Velde, R., Wang, L., Xu, K., Wang, X., and Wen, J.: Blending satellite observed, model simulated, and in situ measured soil moisture over Tibetan Plateau, Remote Sens., 8, 268,doi:10.3390/rs8030268, 2016.

Zhang, H. P., Liu, S. F., Yang, N., Zhang, Y. Q., and Zhang, G. W.: Geomorphic characteristics of the Minjiang drainage basin (eastern Tibetan Plateau) and its tectonic implications: New insights from a digital elevation model study, Island Arc., 15, 239-250,doi:10.1111/j.1440-1738.2006.00524.x, 2006.

Zhang, Y., Li, B., and Zheng, D.: Datasets of the boundary and area of the Tibetan Plateau, Acta Geographica Sinica, 69(Suppl.), 164-168, 2014a.

Zhang, Y., Li, B., and Zheng, D.: Datasets of the Boundary and Area of the Tibetan Plateau, Global Change Data Repository, doi:10.3974/geodb.2014.01.12.V1., 2014b.

Zhao, H., Zeng, Y., Lv, S., and Su, Z.: Analysis of soil hydraulic and thermal properties for land surface modeling over the Tibetan Plateau, Earth Syst. Sci. Data, 10, 1031,doi:10.5194/essd-10-1031-2018, 2018.

Zhao, L., Ping, C.-L., Yang, D., Cheng, G., Ding, Y., and Liu, S.: Changes of climate and seasonally frozen ground over the past 30 years in Qinghai–Xizang (Tibetan) Plateau, China, Glob. Planet. Change, 43, 19-31,doi:10.1016/j.gloplacha.2004.02.003, 2004.

Zheng, D., Van der Velde, R., Su, Z., Wen, J., Wang, X., Booij, M. J., Hoekstra, A. Y., Lv, S., Zhang, Y., and Ek, M. B.: Impacts of Noah model physics on catchment-scale runoff simulations, J. Geophys. Res.: Atmos., 121, 807-832,doi:10.1002/2015JD023695, 2016.

Zhong, M., Duan, J., Xu, H., Peng, P., Yan, H., and Zhu, Y.: Trend of China land water storage redistribution at medi-and large-spatial scales in recent five years by satellite gravity observations, Chinese Sci. Bull., 54, 816-821,doi:10.1007/s11434-008-0556-2, 2009.

Zhuang, R., Zeng, Y., Manfreda, S., and Su, Z.: Quantifying long-term land surface and root zone soil moisture over Tibetan Plateau, Remote Sens., 12, 509,doi:10.3390/rs12030509, 2020.

Page 10: [1] Formatted 李 梦娜 **06/03/2021 10:48:00**

Font color: Auto

Page 10: [1] Formatted 李 梦娜 **06/03/2021 10:48:00**

Font color: Auto

Page 10: [1] Formatted 李 梦娜 **06/03/2021 10:48:00**

Font color: Auto

Page 10: [2] Formatted 李 梦娜 **06/03/2021 10:48:00**

Font color: Auto

Page 10: [2] Formatted 李 梦娜 **06/03/2021 10:48:00**

Font color: Auto

Page 10: [2] Formatted 李 梦娜 **06/03/2021 10:48:00**

Font color: Auto

Page 10: [2] Formatted 李 梦娜 **06/03/2021 10:48:00**

Font color: Auto

Page 10: [2] Formatted 李 梦娜 **06/03/2021 10:48:00**

Font color: Auto

Page 10: [2] Formatted 李 梦娜 **06/03/2021 10:48:00**

Font color: Auto

Page 10: [3] Formatted 李 梦娜 **06/03/2021 10:48:00**

Font color: Auto

Page 10: [3] Formatted 李 梦娜 **06/03/2021 10:48:00**

Font color: Auto

Page 10: [3] Formatted 李 梦娜 **06/03/2021 10:48:00**

Font color: Auto

Page 10: [4] Formatted 李 梦娜 **06/03/2021 10:48:00**

Font color: Auto

Page 10: [4] Formatted 李 梦娜 **06/03/2021 10:48:00**

Font color: Auto

Page 10: [4] Formatted 李 梦娜 **06/03/2021 10:48:00**

Font color: Auto

Page 10: [5] Formatted 李 梦娜 **06/03/2021 10:48:00**

Font color: Auto

Page 10: [5] Formatted 李 梦娜 **06/03/2021 10:48:00**

Font color: Auto

Page 10: [6] Formatted 李 梦娜 **06/03/2021 10:48:00**

Font color: Auto

Page 10: [6] Formatted 李 梦娜 **06/03/2021 10:48:00**

Font color: Auto

Page 10: [6] Formatted 李 梦娜 **06/03/2021 10:48:00**

Font color: Auto

Page 10: [6] Formatted 李 梦娜 **06/03/2021 10:48:00**

Font color: Auto

Page 10: [6] Formatted 李 梦娜 **06/03/2021 10:48:00**

Font color: Auto

Page 10: [6] Formatted 李 梦娜 **06/03/2021 10:48:00**

Font color: Auto

Page 10: [6] Formatted 李 梦娜 **06/03/2021 10:48:00**

Font color: Auto

Page 10: [6] Formatted 李 梦娜 **06/03/2021 10:48:00**

Font color: Auto

Page 10: [6] Formatted 李 梦娜 **06/03/2021 10:48:00**

Font color: Auto

Page 10: [6] Formatted 李 梦娜 **06/03/2021 10:48:00**

Font color: Auto

Page 10: [6] Formatted 李 梦娜 **06/03/2021 10:48:00**

Font color: Auto

Page 10: [6] Formatted 李 梦娜 **06/03/2021 10:48:00**

Font color: Auto

Page 10: [6] Formatted 李 梦娜 **06/03/2021 10:48:00**

Font color: Auto

Page 10: [6] Formatted 李 梦娜 **06/03/2021 10:48:00**

Font color: Auto

Page 10: [6] Formatted 李 梦娜 **06/03/2021 10:48:00**

Font color: Auto

Page 10: [6] Formatted 李 梦娜 **06/03/2021 10:48:00**

Font color: Auto

Page 10: [6] Formatted 李 梦娜 **06/03/2021 10:48:00**

Font color: Auto

Page 10: [7] Formatted 李 梦娜 **06/03/2021 10:48:00**

Font color: Auto

Page 10: [7] Formatted 李 梦娜 **06/03/2021 10:48:00**

Font color: Auto

Page 10: [7] Formatted	**李 梦娜**	**06/03/2021 10:48:00**

Font color: Auto

Page 10: [8] Formatted	**李 梦娜**	**06/03/2021 10:48:00**

Font color: Auto

Page 10: [8] Formatted	**李 梦娜**	**06/03/2021 10:48:00**

Font color: Auto

Page 10: [8] Formatted	**李 梦娜**	**06/03/2021 10:48:00**

Font color: Auto

Page 10: [9] Formatted	**李 梦娜**	**06/03/2021 10:48:00**

Font color: Auto

Page 10: [9] Formatted	**李 梦娜**	**06/03/2021 10:48:00**

Font color: Auto

Page 10: [9] Formatted	**李 梦娜**	**06/03/2021 10:48:00**

Font color: Auto

Page 10: [10] Formatted	**李 梦娜**	**06/03/2021 10:48:00**

Font color: Auto

Page 10: [10] Formatted	**李 梦娜**	**06/03/2021 10:48:00**

Font color: Auto

Page 10: [11] Formatted	**李 梦娜**	**06/03/2021 10:48:00**

Font color: Auto

Page 10: [11] Formatted	**李 梦娜**	**06/03/2021 10:48:00**

Font color: Auto

Page 10: [11] Formatted	**李 梦娜**	**06/03/2021 10:48:00**

Font color: Auto

Page 10: [12] Formatted	**李 梦娜**	**06/03/2021 10:48:00**

Font color: Auto

Page 10: [12] Formatted	**李 梦娜**	**06/03/2021 10:48:00**

Font color: Auto

Page 10: [12] Formatted	**李 梦娜**	**06/03/2021 10:48:00**

Font color: Auto

Page 10: [13] Formatted	**李 梦娜**	**06/03/2021 10:48:00**

Font color: Auto

Page 10: [13] Formatted	**李 梦娜**	**06/03/2021 10:48:00**

Font color: Auto

Page 10: [13] Formatted 李 梦娜 **06/03/2021 10:48:00**

Font color: Auto

Page 10: [13] Formatted 李 梦娜 **06/03/2021 10:48:00**

Font color: Auto

Page 10: [13] Formatted 李 梦娜 **06/03/2021 10:48:00**

Font color: Auto

Page 10: [13] Formatted 李 梦娜 **06/03/2021 10:48:00**

Font color: Auto

Page 10: [14] Formatted 李 梦娜 **06/03/2021 10:48:00**

Font color: Auto

Page 10: [14] Formatted 李 梦娜 **06/03/2021 10:48:00**

Font color: Auto

Page 10: [14] Formatted 李 梦娜 **06/03/2021 10:48:00**

Font color: Auto

Page 10: [15] Formatted 李 梦娜 **06/03/2021 10:48:00**

Font color: Auto

Page 10: [15] Formatted 李 梦娜 **06/03/2021 10:48:00**

Font color: Auto

Page 10: [15] Formatted 李 梦娜 **06/03/2021 10:48:00**

Font color: Auto

Page 10: [16] Formatted 李 梦娜 **06/03/2021 10:48:00**

Font color: Auto

Page 10: [16] Formatted 李 梦娜 **06/03/2021 10:48:00**

Font color: Auto

Page 10: [16] Formatted 李 梦娜 **06/03/2021 10:48:00**

Font color: Auto

Page 10: [16] Formatted 李 梦娜 **06/03/2021 10:48:00**

Font color: Auto

Page 10: [16] Formatted 李 梦娜 **06/03/2021 10:48:00**

Font color: Auto

Page 10: [16] Formatted 李 梦娜 **06/03/2021 10:48:00**

Font color: Auto

Page 16: [17] Deleted 李 梦娜 **05/03/2021 15:35:00**

Page 17: [18] Formatted 李 梦娜 **06/03/2021 10:48:00**

Font color: Auto

Page 17: [19] Deleted	**李 梦娜**	**05/03/2021 15:43:00**

Page 17: [20] Formatted	**李 梦娜**	**06/03/2021 10:48:00**

Font color: Auto

Page 17: [21] Deleted	**李 梦娜**	**05/03/2021 15:46:00**

Page 17: [22] Formatted	**李 梦娜**	**06/03/2021 10:48:00**

Font color: Auto

Page 17: [23] Formatted	**李 梦娜**	**06/03/2021 10:48:00**

Font color: Auto

Page 17: [24] Formatted	**李 梦娜**	**06/03/2021 10:48:00**

Font color: Auto

Page 17: [25] Formatted	**李 梦娜**	**06/03/2021 10:48:00**

Font color: Auto

Page 17: [26] Formatted	**李 梦娜**	**06/03/2021 10:48:00**

Font color: Auto

Page 17: [27] Formatted	**李 梦娜**	**06/03/2021 10:48:00**

Font color: Auto

Page 17: [28] Formatted	**李 梦娜**	**06/03/2021 10:48:00**

Font color: Auto

Page 17: [29] Formatted	**李 梦娜**	**06/03/2021 10:48:00**

Font color: Auto

Page 17: [30] Formatted	**李 梦娜**	**06/03/2021 10:48:00**

Font color: Auto

Page 17: [31] Formatted	**李 梦娜**	**06/03/2021 10:48:00**

Font color: Auto

Page 17: [32] Formatted	**李 梦娜**	**06/03/2021 10:48:00**

Font color: Auto

Page 17: [33] Formatted	**李 梦娜**	**06/03/2021 10:48:00**

Font color: Auto

Page 17: [34] Formatted	**李 梦娜**	**06/03/2021 10:48:00**

Font color: Auto

Page 17: [35] Formatted	**李 梦娜**	**06/03/2021 10:48:00**

Font color: Auto

Page 17: [36] Formatted	**李 梦娜**	**06/03/2021 10:48:00**

Font color: Auto

Page 17: [37] Formatted 李 梦娜 **06/03/2021 10:48:00**

Font color: Auto

Page 17: [38] Formatted 李 梦娜 **06/03/2021 10:48:00**

Font color: Auto

Page 17: [39] Formatted 李 梦娜 **06/03/2021 10:48:00**

Font color: Auto

Page 17: [40] Formatted 李 梦娜 **06/03/2021 10:48:00**

Font color: Auto

Page 17: [41] Formatted 李 梦娜 **06/03/2021 10:48:00**

Font color: Auto

Page 17: [42] Formatted 李 梦娜 **06/03/2021 10:48:00**

Font color: Auto

Page 17: [43] Formatted 李 梦娜 **06/03/2021 10:48:00**

Font color: Auto

Page 17: [44] Formatted 李 梦娜 **06/03/2021 10:48:00**

Font color: Auto

Page 17: [45] Formatted 李 梦娜 **06/03/2021 10:48:00**

Font color: Auto

Page 17: [46] Formatted 李 梦娜 **06/03/2021 10:48:00**

Font color: Auto

Page 17: [47] Formatted 李 梦娜 **06/03/2021 10:48:00**

Font color: Auto

Page 17: [48] Formatted 李 梦娜 **06/03/2021 10:48:00**

Font color: Auto

Page 17: [49] Formatted 李 梦娜 **06/03/2021 10:48:00**

Font color: Auto

Page 17: [50] Formatted 李 梦娜 **06/03/2021 10:48:00**

Font color: Auto

Page 17: [51] Formatted 李 梦娜 **06/03/2021 10:48:00**

Font color: Auto

Page 17: [52] Formatted 李 梦娜 **06/03/2021 10:48:00**

Font color: Auto

Page 17: [53] Formatted 李 梦娜 **06/03/2021 10:48:00**

Font color: Auto

Page 17: [54] Formatted 李 梦娜 **06/03/2021 10:48:00**

Font color: Auto

Page 17: [55] Formatted 李 梦娜 **06/03/2021 10:48:00**

Font color: Auto

Page 17: [56] Formatted 李 梦娜 **06/03/2021 10:48:00**

Font color: Auto

Page 17: [57] Formatted 李 梦娜 **06/03/2021 10:48:00**

Font color: Auto

Page 17: [58] Formatted 李 梦娜 **06/03/2021 10:48:00**

Font color: Auto

Page 17: [59] Formatted 李 梦娜 **06/03/2021 10:48:00**

Font color: Auto

Page 17: [60] Formatted 李 梦娜 **06/03/2021 10:48:00**

Font color: Auto

Page 17: [61] Formatted 李 梦娜 **06/03/2021 10:48:00**

Font color: Auto

Page 17: [62] Formatted 李 梦娜 **06/03/2021 10:48:00**

Font color: Auto

Page 17: [63] Formatted 李 梦娜 **06/03/2021 10:48:00**

Font color: Auto

Page 17: [64] Formatted 李 梦娜 **06/03/2021 10:48:00**

Font color: Auto

Page 17: [65] Formatted 李 梦娜 **06/03/2021 10:48:00**

Font color: Auto

Page 17: [66] Formatted 李 梦娜 **06/03/2021 10:48:00**

Font color: Auto

Page 18: [67] Formatted 李 梦娜 **06/03/2021 10:48:00**

Font color: Auto

Page 18: [68] Formatted 李 梦娜 **06/03/2021 10:48:00**

Font color: Auto

Page 18: [69] Formatted 李 梦娜 **06/03/2021 10:48:00**

Font color: Auto

Page 18: [70] Formatted 李 梦娜 **06/03/2021 10:48:00**

Font color: Auto

Page 18: [71] Formatted 李 梦娜 **06/03/2021 10:48:00**

Font color: Auto

Page 18: [72] Formatted 李 梦娜 **06/03/2021 10:48:00**

Font color: Auto

Page 18: [73] Formatted **李 梦娜** **06/03/2021 10:48:00**

Font color: Auto

Page 18: [74] Formatted **李 梦娜** **06/03/2021 10:48:00**

Font color: Auto

Page 18: [75] Formatted **李 梦娜** **06/03/2021 10:48:00**

Font color: Auto

Page 18: [76] Formatted **李 梦娜** **06/03/2021 10:48:00**

Font color: Auto

Page 18: [77] Formatted **李 梦娜** **06/03/2021 10:48:00**

Font color: Auto

Page 18: [78] Formatted **李 梦娜** **06/03/2021 10:48:00**

Font color: Auto

Page 18: [79] Formatted **李 梦娜** **06/03/2021 10:48:00**

Font color: Auto

Page 18: [80] Formatted **李 梦娜** **06/03/2021 10:48:00**

Font color: Auto

Page 18: [81] Formatted **李 梦娜** **06/03/2021 10:48:00**

Font color: Auto

Page 18: [82] Formatted **李 梦娜** **06/03/2021 10:48:00**

Font color: Auto

Page 18: [83] Formatted **李 梦娜** **06/03/2021 10:48:00**

Font color: Auto

Page 18: [84] Formatted **李 梦娜** **06/03/2021 10:48:00**

Font color: Auto

Page 18: [85] Formatted **李 梦娜** **06/03/2021 10:48:00**

Font color: Auto

Page 18: [86] Formatted **李 梦娜** **06/03/2021 10:48:00**

Font color: Auto

Page 18: [87] Formatted **李 梦娜** **06/03/2021 10:48:00**

Font color: Auto

Page 18: [88] Formatted **李 梦娜** **06/03/2021 10:48:00**

Font color: Auto

Page 18: [89] Formatted **李 梦娜** **06/03/2021 10:48:00**

Font color: Auto

Page 18: [90] Formatted 李 梦娜 06/03/2021 10:48:00

Font color: Auto

Page 18: [91] Formatted 李 梦娜 06/03/2021 10:48:00

Font color: Auto

Page 18: [92] Formatted 李 梦娜 06/03/2021 10:48:00

Font color: Auto

Page 18: [93] Formatted 李 梦娜 06/03/2021 10:48:00

Font color: Auto

Page 18: [94] Formatted 李 梦娜 06/03/2021 10:48:00

Font color: Auto

Page 18: [95] Formatted 李 梦娜 06/03/2021 10:48:00

Font color: Auto

Page 18: [96] Formatted 李 梦娜 06/03/2021 10:48:00

Font color: Auto

Page 18: [97] Formatted 李 梦娜 06/03/2021 10:48:00

Font color: Auto

Page 18: [98] Formatted 李 梦娜 06/03/2021 10:48:00

Font color: Auto

Page 18: [99] Formatted 李 梦娜 06/03/2021 10:48:00

Font color: Auto

Page 18: [100] Formatted 李 梦娜 06/03/2021 10:48:00

Font color: Auto

Page 18: [101] Formatted 李 梦娜 06/03/2021 10:48:00

Font color: Auto

Page 18: [102] Formatted 李 梦娜 06/03/2021 10:48:00

Font color: Auto

Page 18: [103] Formatted 李 梦娜 06/03/2021 10:48:00

Font color: Auto

Page 18: [104] Change Unknown

Field Code Changed

Page 18: [105] Formatted 李 梦娜 06/03/2021 10:48:00

Font color: Auto

Page 18: [106] Deleted 李 梦娜 05/03/2021 15:55:00

Page 20: [107] Deleted 李 梦娜 05/03/2021 15:36:00